



RESEARCH

Seismological study around the Enguri dam reservoir (Georgia) based on old catalogs and ongoing monitoring

Nasim Karamzadeh · Nino Tsereteli ·
Emmanuel Gaucher · Nazi Tugushi ·
Tamar Shubladze · Otar Varazanashvili ·
Andreas Rietbrock

Received: 11 March 2023 / Accepted: 13 October 2023
© The Author(s) 2023

Abstract In the frame of the DAMAST (Dams and Seismicity) project, we deployed a dense high-fidelity seismological real-time network to investigate in detail the spatio-temporal seismicity distribution around the Enguri high dam, situated in the greater Caucasus in western Georgia. We aim at recording the weak seismicity in a 10 km distance around the dam structure. To lower the detection threshold by reducing the ambient background noise, we installed four seismic stations in shallow (ca. 20 m) and deep boreholes. From these stations, KIT1 with a depth of ca. 250 m is the deepest seismological station in Georgia. In this paper, we characterize the seismicity recorded by the local seismic network from October 2020 to July 2022. To have a better historical picture of the seismic activity, especially since the dam construction and initial operations, re-processing of the old seismological catalogs was carried out. This required digitizing the paper-only catalog

copies prior to relocation. We finally obtain a uniform catalog for the Enguri region to characterize the seismicity and start investigating its possible relationship with the exploitation of the dam reservoirs.

Keywords Active faults · Earthquake catalog · Ingirishi fault · Local seismic network · Old seismic data · Seismicity monitoring

1 Introduction

The study region is centered on the Enguri dam, in western Georgia, and is located in an area prone to high seismic activity with moderate intensity, i.e., greater Caucasus, about 50 km east of the Black Sea (see Fig. 1). The dam is the main part of the Enguri hydroelectric power plant (HPP), which is partly located in Abkhazia region and plays an important role in power supply for Georgia. With 271 m in height, the Enguri dam is one of the world's highest arch dams. The dam reservoir with an average volume of one billion cubic meters and an annual water level variation of about 100 m in close vicinity of active faults, makes the area a very interesting case study for reservoir-induced seismicity and the study of the interaction between dam reservoirs and faults (Braun et al. 2018; Gupta 1992; Stabile et al. 2014).

The installation of a seismic network around the Enguri dam began in 1972 prior to the temporary operation of the dam in 1978. The first induced earthquake recorded

N. Karamzadeh (✉) · A. Rietbrock
Geophysical Institute, Karlsruhe Institute of Technology,
Hertzstr. 16, 76187 Karlsruhe, Germany
e-mail: nasim.karamzadeh@kit.edu

A. Rietbrock
e-mail: andreas.rietbrock@kit.edu

N. Tsereteli · N. Tugushi · T. Shubladze · O. Varazanashvili
M. Nodia Institute of Geophysics, Tbilisi State University,
1, Alexidze str., 0160 Tbilisi, Georgia
e-mail: nino_tsereteli@tsu.ge

E. Gaucher
Institute of Applied Geosciences, Karlsruhe Institute
of Technology, Adenauerring 20b, 76131 Karlsruhe, Germany

by that network took place in 1979 when the dam reservoir was filled for the first time. The magnitude of the main shock was M_s 4.3 and about 80 aftershocks were observed over several months. In 1992, the maintenance of the seismic network around the Enguri dam stopped. In July 2010, however, another earthquake of M_s 4.3, recorded by the National Seismic Network of Georgia, took place but the related aftershocks could not be recorded, due to poor National network coverage in the area.

The old catalog of seismicity provided a great resource to investigate the initial changes imposed in the regional seismicity as a result of the dam's early-day operations. The analysis of the old catalog indicates the dramatic increase of seismic activity in the initial stages of reservoir filling and decrease of it in subsequent years (Peinke et al. 2006). Further studies of the changes in regional seismicity as a result of water level variation revealed evidence of annual oscillation of seismicity with the dam water level variations (Chelidze et al. 2019, 2021; Matcharashvili et al. 2013; Peinke et al. 2006; Telesca et al. 2012, 2015).

The present paper contributes from the integration and harmonization of old and recent seismological data to increase our knowledge of the seismicity induced by high dams and in the assessment of seismic hazards related to hydroelectrical power generation in general. We show the current state of seismicity close to the Enguri dam reservoir, as recorded by the local modern seismic network installed in the framework of the DAMAST project and operating for about 2 years. The newly installed local seismic network includes four stations at the surface, 3 stations in shallow boreholes, and one in a deep borehole. It focuses mainly on the weak seismicity within a 10 km distance from the dam structure and the Ingirishi fault. The current seismicity map indicates activity on existing faults; however, the detailed identification of the active faults branches, geometry and slip mechanism, and the possible link between seismicity and the dam-reservoir water level changes are subjects to ongoing studies. Nevertheless, for the biggest event that occurred inside the network, the fault plane solution is calculated using the first arrivals polarities and S-phase to P-phase amplitude ratio. Besides the real-time monitoring of the seismicity around the dam, we digitized and re-processed the old analog data using a standard numerical location method to improve the image of the seismicity especially at, during, and shortly after the dam construction.

1.1 Seismotectonic of Enguri area

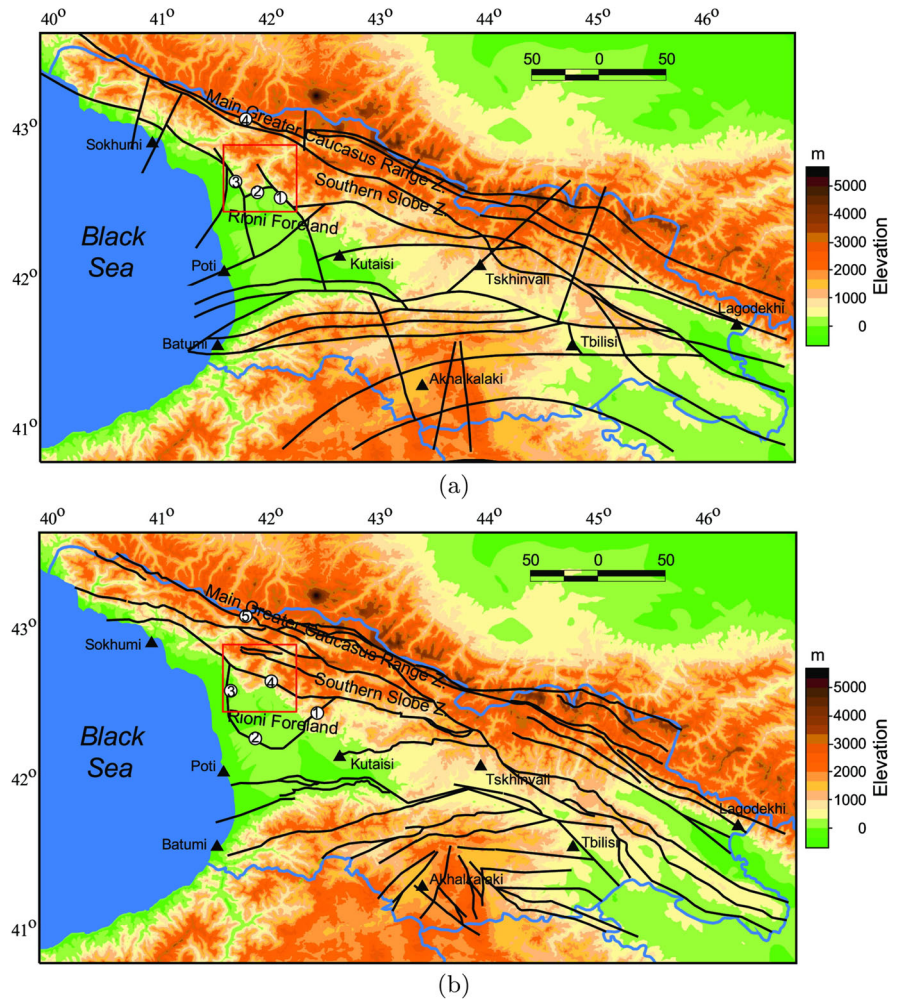
Tectonic and geodynamics of Georgia, as a part of the Caucasus region, were influenced by the continental-continental collision of the Eurasian and Afro-Arabian plates in the Mediterranean belt (Alpine-Himalayan), at the interface of the European and Asian segments. The conversion of the two plates resulted in an intra-continental mountain belt in the Caucasus region, with active structures and topography, i.e. high mountain ranges of the Great and Lesser Caucasus, intermontane lowlands of the Transcaucasus, and volcanic highlands, intensely being developed since the late Sarmatian (7 Ma) (Adamia et al. 1981, 2010, 2017; Allen et al. 2004; Banks et al. 1998; Dewey et al. 1973; Jackson et al. 1997; Khain 1975; Martin et al. 2010; McClusky et al. 2000; Mosar et al. 2010; Pasquarè et al. 2011; Pearce et al. 1990; Reilinger et al. 2006; Smith 1971; Sosson et al. 2010; Tan and Taymaz 2006; Tibaldi et al. 2017a, b, 2018a, 2021). The tectonic deformation of the region is mainly formed by the wedge-shaped rigid Arabian block motion, which intensively indents into the relatively mobile area (Adamia et al. 2017; Allen et al. 2003; Berberian and Yeats 1999; Jackson and McKenzie 1988; Jackson et al. 1997; Koçyiğit et al. 2001; McClusky et al. 2000; Okay and Sahinturk 1997; Vincent et al. 2005; Yilmaz et al. 1997). Consequently, all structural-morphological lines represent a clear arcuate northward convex pattern following the contours of the Arabian block (Allen et al. 2003; Axen et al. 2001; Reilinger et al. 2006). However, farther north, the geometry of the fold-and-thrust belt revolves; for instance, the Achara-Trialeti structure appears in an Eastward-Westward orientation. The Great Caucasian old-and-thrust belt extends in a WNW-ESE (300–120°) direction, while the chains of Neogene-Quaternary volcanoes in the Lesser Caucasus are oriented in a submeridional (N-S) direction. The submeridional compression reaches its maximum within the central segment of the Caucasus, along a line running through the central part of the Transcaucasus. This line actually represents the watershed between the basins of the Black Sea and the southern Caspian Sea. Westward of this line, the escape of the central Anatolia plate takes place. So, the territory of the Black Sea experiences weak submeridional compression. Apparently, the same conditions also exist eastward of the line of maximal compression in the territory of the Kura foreland and Talesh in southeastern Caucasus (Adamia et al.

2008; Koçyiğit et al. 2001; Varazanashvili et al. 2011). The Caucasus region is subjected to not only S-N, but also E-W compression. Since it is directly adjacent to the eastern Black Sea on the west and the Caspian Sea on the east, each of which with a suboceanic high-density crust that hampers lateral tectonic escape of the western and eastern Caucasus, respectively. The compression is attenuated to the east and west from the central segments of the Caucasus like butterfly wings. According to the seismological, paleoseismological, and GPS data, convergence between the Eurasian and African-Arabian plates is still active, causing deformation within the mountain belt and in surrounding regions (Adamia et al. 2017; Alizadeh et al. 2016; Allen et al. 2004; Avagyan et al. 2010; Jackson et al. 1997; Kadirov et al. 2008, 2015, 2012; Koçyiğit et al. 2001; Pasquarè et al. 2011; Rebai et al. 1993; Reilinger et al. 2006; Sokhadze et al. 2018; Tan and Taymaz 2006; Tibaldi et al. 2017a, b, 2018b; Tsereteli et al. 2016b). Based on the GPS data, the convergent rate is up to 30 mm/year (DeMets et al. 1990, 1994; Reilinger et al. 2006; Triep et al. 1995). Although the induced tectonic stress by the northward motion of the Arabian plate is mainly absorbed in the Periarabian Ophiolitic Suture Zone and in the Zagros fold-thrust belts, the stress is propagated towards the Central Caucasus and causes crustal shortening and causes the convergent rate of up to 10 mm/year and 4 mm/year across the Lesser Caucasus and Greater Caucasus, respectively. The rate of convergence between the Lesser and Greater Caucasus, in fact, decreases from about 14 mm/year in the Kura Basin to about 4 mm/year in the Rioni basin (Aktuğ et al. 2013; Guliev et al. 2002; Kadirov et al. 2012; McClusky et al. 2000; Reilinger et al. 1997, 2006; Shevchenko et al. 1999; Sokhadze et al. 2018). The major geodynamic activity of the region results in the occurrence of frequent moderate to strong earthquakes. The map of known faults in Georgia is mostly based on the offset of main geological units. According to the geological, tectonic and seismicity maps some faults are classified as Quaternary faults. Figure 1a and b present two main active fault models developed by Caputo et al. (2000) and Adamia et al. (2008, 2010). Although these two models show significant differences, the orientation of the active faults in the region in both models is consistent and follows four main directions, which are Caucasian trend from WNW/W to ESE/E, E-W trends, and two transversal trends in NE-SW and NW-SE directions. The

focal mechanism solution of the moderate and strong earthquakes along active faults indicates three stress regimes, i.e., strike-slip, thrust, and transpressional fault zones. The Caucasian-strike active faults are represented by thrust mechanism in the western and central part of the Great Caucasus and transpressional and strike-slip faults in the eastern part, where the strike-slip mechanism is dominant (Adamia et al. 2008, 2017; Jackson and McKenzie 1988; Philip et al. 1989; Tan and Taymaz 2006; Tibaldi et al. 2018a, 2021; Tsereteli et al. 2016a, b). Most transversal active faults are located in the Javakheti volcanic highland in South Georgia, which is a young tectonic unit formed during the Neogene-Quaternary era with active faults mainly in left-lateral and right-lateral motions where the seismicity includes shallow depth small earthquakes, up to 5 km depth with a local magnitude of below 2.5 M_l (Tsereteli et al. 2012).

From a geotectonic point of view, the Enguri hydroelectric power plant area is represented by the three main tectonic units (see Fig. 1) with a different history of geological development and structure. The tectonic units include the Main Range Zone of the Greater Caucasus with a predominance of significant newest uplifts; the Southern Slope Zone of the Greater Caucasus and Georgian Block represented at this site by intermountain Rioni Foreland (Caputo et al. 2000; Gamkrelidze 1966; Murusidze 1980). The dam structure is located in the connection of the Southern Slope Zone of the Great Caucasus and Georgian Block (Fig. 1). According to the detailed geo-engineering and seismic-acoustic studies, the base of the dam is composed of Cretaceous rocks, mainly Barremian limestones, the layers of which dip at an angle of 50 to 60° and are characterized by highly developed fracturing (Murusidze and Lursmanashvili 1962). Based on Caputo et al. (2000) in the zone where the arch dam is located, due to the uplift of the Southern Slope Zone with simultaneous pressure of the masses to the south, the old faulting happened and new transpressional active faults appeared. The closest active faults to the Enguri dam are the Gagra-Java active fault to the south with NE-SW direction, the Tskhakaia-Tsaishi active fault to SW of the dam with NW-S direction, and Vartsikhe-Gegechkori active fault with NW-SE direction (Fig. 1a). However, according to Adamia et al. (2008) westward escape of the western Transcaucasus led to the formation of the seismoactive structure represented by the chain of Gali, Zugdidi, Khobi, Eki, and Abedati anticlines that fully delineates the Odishi

Fig. 1 Map of active faults in Georgia **a** based on Caputo et al. (2000) **b** based on Adamia et al. (2008, 2017) (The black lines. The main seismotectonic zones around the study area (red rectangle) are indicated on both maps. The blue line represents the country borders. Faults indicated with numbers on plot (a) are 1: Vartsikhe-Gegechkori, 2: Gagra-Java, 3: Tskhakaia-Tsaishi, 4: Main Trust of Greater Caucasus; and faults marked with numbers on plot (b) are 1: Odishi (segment Martvili), 2: Odishi (segment Khobi), 3: Odishi (segment Achigvara), 4: Racha-Lethkhumi, 5: Main Trust of Greater Caucasus



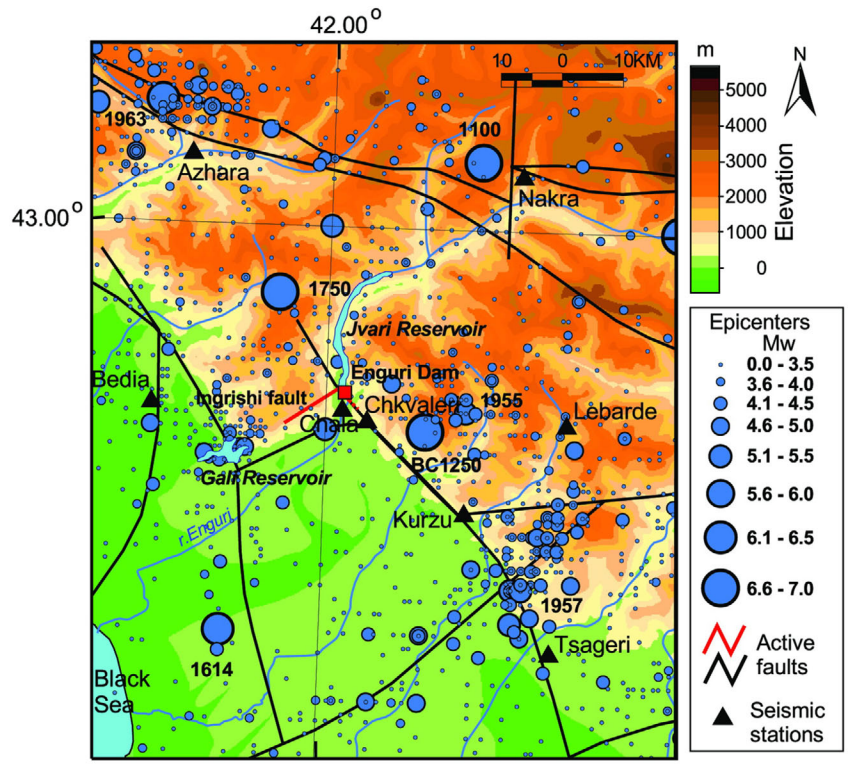
Piggyback basin by Odishi active fault contains several segments with different cinematics: left-lateral reverse Martvili segment, reverse Khobi segments, right-lateral reverse Achigvara segments. The closest (up to 2 km) active fault to the structure of Enguri dam is the Racha-Lethkhumi (segment Mukhuri) reverse active fault to the north (Fig. 1b).

In Fig. 2a and b, active faults around Enguri dam are plotted, where Ingirishi fault which passes in direct proximity to the dam is shown with red line (Mastitsky and Jigauri 1974). According to the previous geological studies, the Ingirishi fault, since the Middle Pliocene age, was not tectonically active; the seismic activity close to the dam structure is recognized to be insignificant, according to the old seismic network (Murusidze 1980). In addition, the most seismically active faults

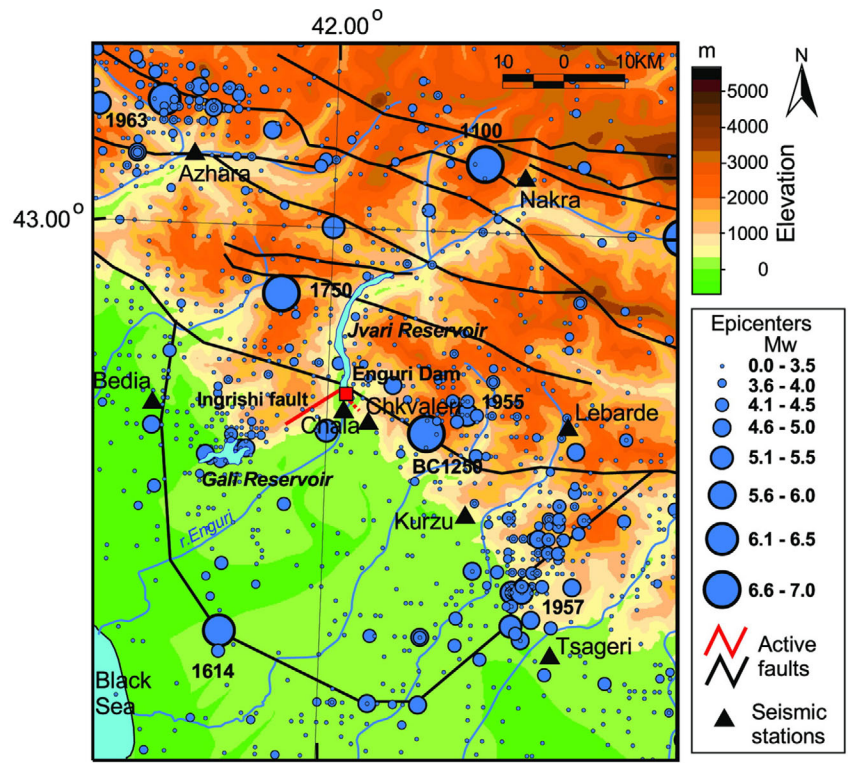
in the area relate to the north of Enguri dam to the Main Trust of Great Caucasus by Caputo et al. (2000) and Adamia et al. (2008, 2017) (Fig. 2a and b) and to the Gagra-Gorabi active reverse faults by Adamia et al. (2008, 2017) that show several reverse active faults crossing the Enguri dam reservoir.

According to the historical earthquake studies (Varazanashvili et al. 2018), Western Georgia has been seismically active and a number of destructive earthquakes as strong as M_w 6.0 to 7.0 occurred in the area before 1900, for example, the Kvira earthquake in 1250 BC close to the dam with M_w 6.9, the Nenskra-Abakura event in 1100 in the north with a magnitude of M_w 6.9, Tsaishi event in 1614 with a magnitude of M_w 6.1, and the Akiba earthquake in 1750 with a magnitude of M_w 6.9.

Fig. 2 Map of active faults around Enguri dam area **a** Caputo et al. (2000) **b** Adamia et al. (2008, 2017) On these maps, the black lines are faults and the blue lines represent rivers. The seismicity depicted in the background (blue circles) is related to the old original catalog. The Ingirishi fault segment which is only recognized in literature (Murusidze 1980) is plotted in red on both maps



(a)



(b)

2 Old seismic network and seismicity

Regular instrumental seismological observation in western Georgia has been carried out since 1937 when the first seismic station was installed in Zugdidi city. However, until 1957 only mechanical seismographs with rather low sensitivity were operating at that station; therefore, the possibility of recording weak earthquakes at this station was very limited. In 1957–1970, six seismic stations were installed in the region (Martvili/Gegechkori, Tsebelda, Oni, Khaishi, Saberio, and Tkibuli). Nevertheless, monitoring weak earthquakes ($\leq M_w 3.5$) did not improve in this period because two of the stations (Saberio and Khaishi) operated irregularly, while the Gegechkori and Zugdidi stations had low sensitivity. Eleven seismic stations have been installed from 1972 to 1980 (Fig. 2 and Table 1). Two of them were located in the highlands of western Georgia, three of them along the Utvir fault of the Main Thrust of Great Caucasus-Gagra-Gorabi, one station was located along Odishi active faults and the remaining ones were located along the Racha-Lechkumi (Gagra-Mukhuri) fault passing near Enguri dam (Fig. 1). All stations were equipped with the same standard seismometers designed for regional seismic stations, recording typical three channels and one coarsened channel (Murusidze 1980; Papalashvili 1981). It should be noted that since the mid90s, due to political and socio-economic changes that have taken place in Georgia, the operation of the local seismic network stopped, and unfortunately, from 1990 until 2019 information about the seismicity of the area comes

only from the Georgian national network. The waveforms of the old network before 2006 are not available anymore for re-processing and only an analog catalog and a bulletin for some events exist. The bulletins include amplitude, the first arrival of P- and S-phases, first motion polarities, and events locations obtained using a basic circle-and-cord and fixed depth approach. Figure 2 shows the seismicity of the area based on the old catalog, including the historical and instrumental earthquakes, and the faults inside the study area.

The filling of the Enguri reservoir began in April 1978. Water level variation from the beginning of the exploitation to 2013 is plotted in Fig. 3a. Enguri reservoir is connected to the Gali reservoir by a 16 km pressure-derivation tunnel (see Fig. 2), which is the second reservoir of the Enguri hydroelectrical power plant to regulate the flow of the Enguri River. As we can see in Figs. 2 and 3b, clustered and scattered earthquakes in the area occurred even before the reservoirs were filled. However, the cluster of earthquakes in 1961 was located in the southeast of the dam about 50 km away. After the initial dam reservoir impoundment, the number of earthquakes increased, and, in December 1979, this process was completed by a series of Rechkhi earthquakes along the Gali water reservoir. The cluster is composed of two main events of $M_w 4.9$ ($M_s 4.2$) and $M_w 5.0$ ($M_s 4.3$), foreshocks, and more than a hundred aftershocks that lasted more than one year. In 2010, another earthquake with $M_w 4.9$ ($M_l 4.6$) took place along the Gali reservoir. These events are discussed in Tibaldi et al. (2017a).

Table 1 Seismic stations of the Enguri HPP area, installed during the period 1972–1980

Station	Installation date (year)	Latitude	Longitude	Elevation (m)	Sensor
Azhara	1972	43.105	41.716	605	SKM-3
Ambrolauri	1980	42.518	43.150	544	SKM-3
Bedia	1973	42.736	41.650	265	SKM-3
Chala	1973	42.733	42.033	315	SKM-3
Chkvaleri	1973	42.717	42.083	385	SKM-3
Dgnorisia	1979	42.467	42.833	910	VEGIK
Kurzu	1973	42.583	42.283	313	SKM-3
Lebarde	1973	42.717	42.483	1530	SKM-3
Mestia	1974	43.033	42.717	1441	SKM-3
Nakra	1974	42.383	42.383	1330	SKM-3
Tsageri	1976	42.380	42.460	524	SKM-3

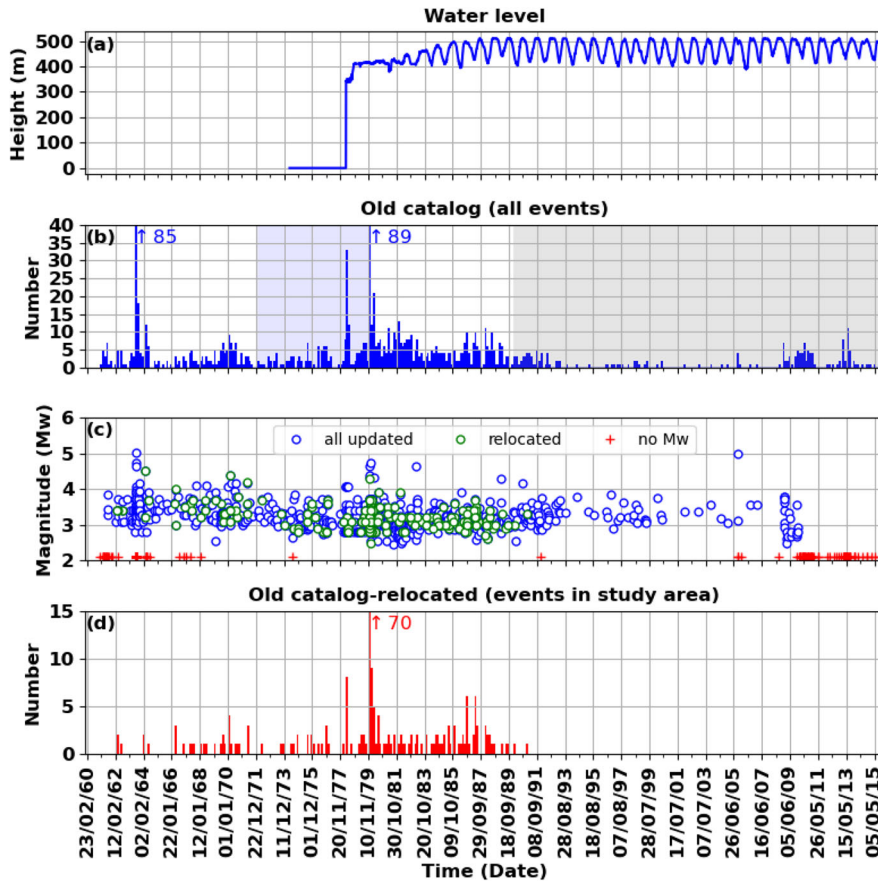


Fig. 3 **a** The water level change at the Enguri dam reservoir. Histograms **b** and **d** show the temporal variation of seismicity according to the old catalog, the length of each bin is 3 months, **b** shows the seismicity observed in a bigger area (Fig. 2), and the **d** shows the relocated old catalog in the study area (inside the red rectangles in Fig. 1) **c** shows the magnitude of all events (M_w) (blue) and relocated events (green) and events without M_w estimation are indicated by red plus signs. The vertical axes are short-

ened both in **(b)** and **(d)** to adapt to the diagram’s major range. The out-of-range values for three peaks are indicated beside up-arrows. The blue background in **b** shows the time that the 11 stations of Enguri old local network started to operate and added to the old 6-station network. The gray background indicates the time that only stations of the Georgian national seismic network were operating

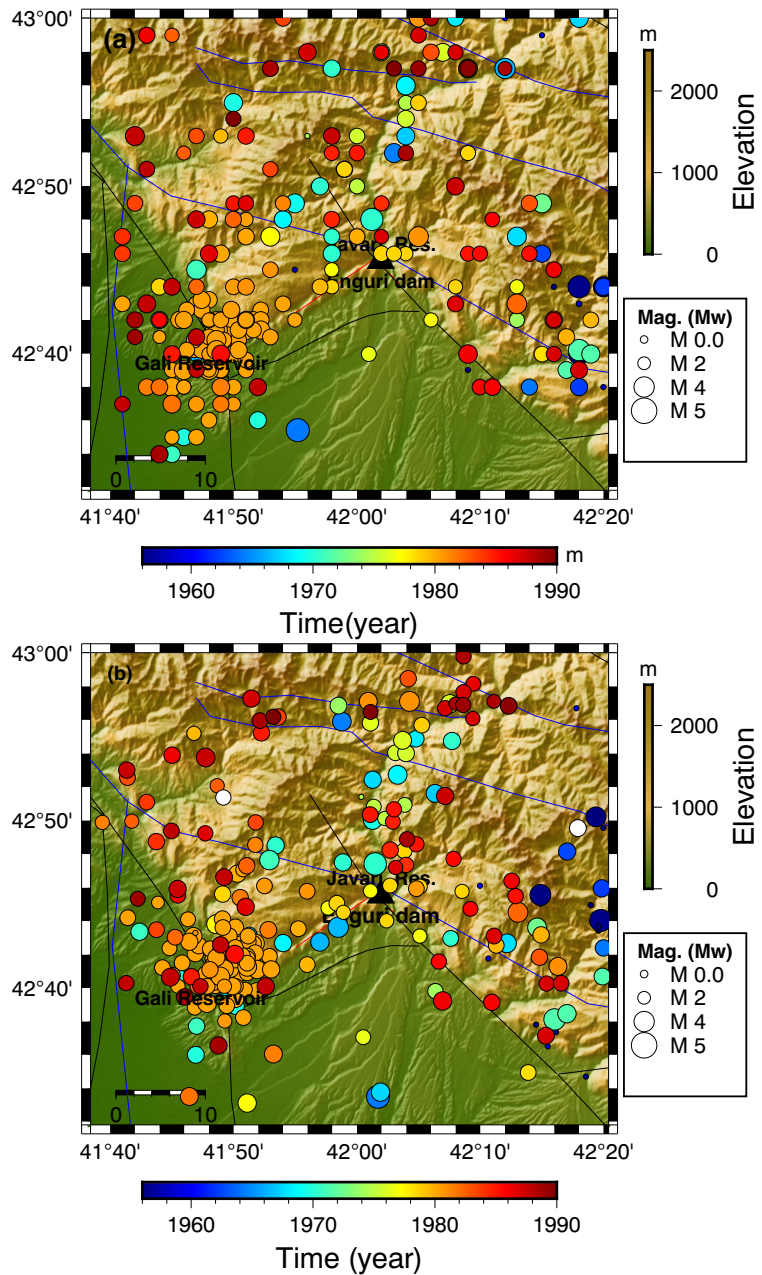
Table 2 1D velocity model used for event location (Murusidze 1987), $V_p/V_s = 1.71$

Depth (km)	P-phase velocity (km/s)
0	4.2
4	5.5
20	6.2
30	6.2
49	8.2

3 Updating the old catalog

The old catalog includes location parameters of 475 events (within a 50-km length frame), while bulletin data is available for only 252 events. The location of those 252 events is updated in this study, employing the old analog bulletin data and the HYPO-71 program (Lee 1975). The relocation procedure using digitized old bulletin and selection of the best velocity model (Table 2) are explained in detail in Tsereteli et al. (2012) and Tsereteli et al. (2016b). Figure 4 shows the updated locations, white circles correspond to loca-

Fig. 4 Seismicity map according to the old catalog, **a** before catalog update, **b** after the catalog update. The color map shows the event's origin time, and circles are sized according to the event's magnitude, however, $M_w = 0$ means that M_w is not estimated. On this map the black and blue lines are faults already introduced in Fig. 2, based on Adamia et al. (2008, 2017) and Caputo et al. (2000), respectively



tions reported in the old catalog and the red ones to the relocation, the colorbar shows the origin time, and circles are sized according to the magnitude of events. In both plots, the magnitude scale of events is M_w . The event magnitudes were unified by conversion equations based on national data developed recently by Onur et al. (2019) and Tibaldi et al. (2020) as well as by regional conversion equations (Zare et al. 2014) for those magnitudes without national conversion equations.

It should be noted that, from 1960 to 2003, in Georgia and the entire Caucasus region, earthquakes magnitude has been estimated in terms of surface waves magnitude M_s or M_{LH} (Russian surface-wavescale) for moderate to strong earthquakes ($M_s \geq 4.0$). For these events regional calibration curves were used. For small and moderate earthquakes whenever the direct determination of M_s was impossible, the size of events were estimated by energy class (K) and conversion equa-

tion $M_s = 0.56K - 2.2$ (Rautian 1964) was employed. Following Rautian (1964), it is accepted that coda magnitude M_c and the surface wave magnitude (M_s) are of the same scale, i.e., $M_c = M_s$, as in many cases coda magnitude was reported in the old catalog. For cases with M_b or M_{PV} (magnitude estimated from the vertical component of P-waves), an empirical correlation formula $M_{PV} = 0.63M_s + 2.5$ was considered. So, until 2003 earthquake catalog for Georgia and Caucasus was unified to surface magnitude M_s . Since 2004, because of the reorganization of the Georgian seismic network, only local magnitude values (M_L or M_l) were calculated for recorded earthquakes (and hardly ever M_c and M_b values in some cases), accordingly, M_w was calculated only for earthquakes with M_L larger than 4.5 (Adamia et al. 2010; Tsereteli et al. 2016b). Comparing original (Fig. 4a) and updated (Fig. 4b) event's locations, one can see that in the old catalog locations appear to be aligned in vertical or horizontal lines indicating a 2-D grid spacing (due to employed simple location technique), while in the updated version events are distributed without any grid-related pattern and could freely form any arbitrary-shaped clusters. In addition, the size of the cluster in the vicinity of the Gali reservoir is smaller and less elongated to the southeast direction after the relocation. In Fig. 3c, the magnitude of events is illustrated in the same time sequence as the other plots in Fig. 3, where the blue circles are all updated magnitudes, green circles are updated magnitude of the relocated events and red plus signs are those events without M_w magnitude conversion possibility. The old catalog magnitude of completeness for all updated magnitudes is about M_w 2.7, and for the relocated events in the region is about M_w 3. In Fig. 3d, the temporal variation of the relocated seismicity is plotted. Figure 5 summarizes the improvement of the old catalog, by showing the event depth distribution before (a) and after (b) relocation and update of the epicentral location (km). It should be noted that in the old catalog events location error is not available and events are categorized in different classes according to the accuracy of epicentral location. The events related to the study area are classified as class C indicating the epicentral error of about 15 km. Until 2000, focal depth was determined by the Wadati method and by intersection of the Levitskaia-Lebedeva travel-time curve, and the error in depth estimation varied from 10 to 20 km. While the most frequent estimation of depth is 25 km in the old catalog, the relocated event's depths

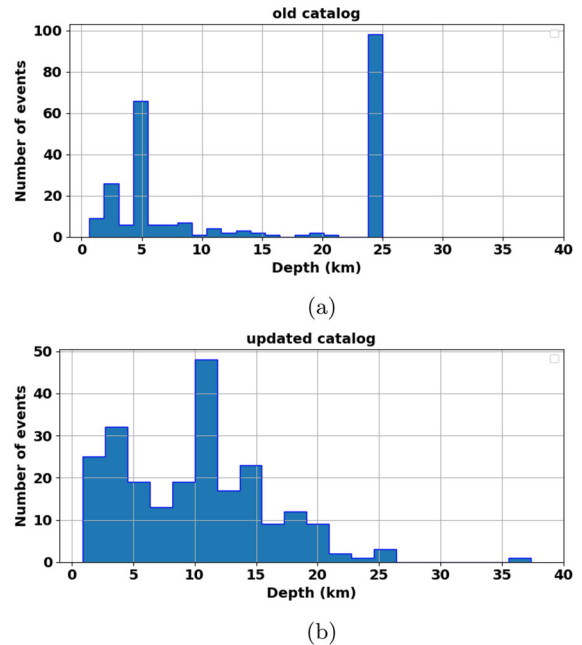


Fig. 5 Number of earthquakes vs. depth **a** before relocation **b** after relocation

are more distributed in shallower depth of less than 15 km and the most frequent depth is 10 km. Accordingly, the origin times and epicentral locations are corrected up to 4 min and 25 km, respectively. In Fig. 6, histogram of relocated events RMS, location error and azimuthal gap are plotted. The majority of events are relocated with RMS values between 0.2 and 0.4 s, horizontal and vertical location errors are less than 2 km, and the most frequent azimuthal gap of the events is about 150 degree.

The pattern of the relocated events shows (Fig. 4b) that earthquakes of magnitude above M_w 3.5 are located all over the area and create a seismic background of the territory. Nevertheless, seismicity along the Gali reservoir is denser than around the dam. In addition, events with a magnitude of above M_w 3.6 are located mainly along the known and identified faults on geological maps. Almost all events are shallower than 25 km, with 12 km as the most frequent depth and a second peak close to 4 km. Based on that, two main active seismogenic zones can be distinguished in the study area.

The first, most seismically active zone is located along the Main Trust of the Great Caucasus fault (Caputo et al. 2000) or Gagra-Gorabi active faults (Adamia et al. 2008, 2017) noted above. The epicenters of the

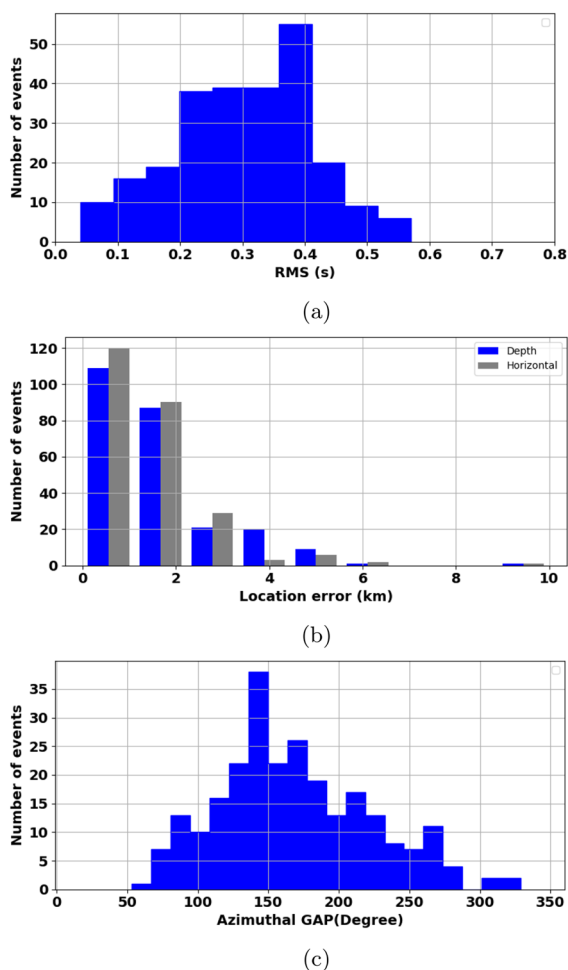


Fig. 6 Histogram of the updated catalog **a** RMS, **b** location error, and **c** Azimuthal gap

strongest earthquakes in western Georgia are located in this zone. It should be noted that since 1955, after improving the seismological station in western Georgia, more seismic activity has been recorded in this zone, and, in 1963, the well-known Chkhalta earthquake with M_w 6.4 occurred within its boundaries, and earlier in 1100, the historical Nenskra-Abakura is related to this zone (see Fig. 1). The second zone is located along the so-called Gagra-Mukhuri fault (Adamia et al. 2008, 2017). In the eastern part of this zone, in 1991, the destructive Ratcha earthquake with M_w 6.9 occurred whereas earlier, in BC 1250 (see Fig. 1), the historical Kvira earthquake occurred. This zone could be of great importance for earthquake hazards associated with the Enguri HPP dam since the indicated fault passes close to it.

4 Enguri current seismic network

We designed an eight-station local seismic network to record weak seismicity in 10 km around the dam, with good coverage and high sensitivity around Ingirishi fault segments. The final layout of the installed network, including stations installed at the surface and boreholes, is shown in Fig. 7. Each online station is equipped with a centaur data logger, router, and SIM card. The stations KIT1 and HPP are connected to AC power, whereas power is provided by solar panels in combination with batteries for the other stations. At stations, GULB, KET1, and BRID, Kinematics MBB-2 sensors are installed, while the other stations are equipped with Nanometrics Trillium compact posthole 20s, and in station HPP in Abkhazia, a 3-D Geophone PE-6/B is running. The depth of the shallow borehole stations, i.e., DOG, BUFF, and NIKA, is between 17 and 19 m, and station KIT1, with a 250-m depth, is the deepest seismic station currently running in Georgia. The network installation was performed in three main stages, October 2020, December 2020, and September 2021. Figure 8 indicates the data availability of each station. For most stations, data has been continuously recorded and transmitted since the installation time, however, data gaps due to technical reasons happened at stations KIT1 (for circa 5 months), GULB, and

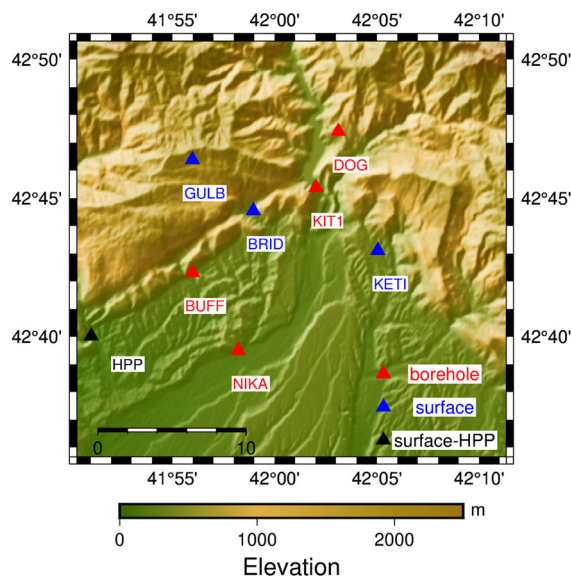
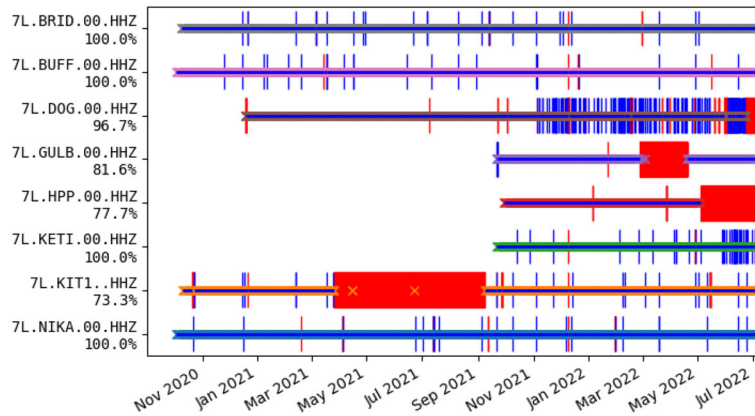


Fig. 7 Location of the local seismic stations. Deep borehole (KIT1) at 250 m, and the shallow boreholes at 17–19 m depth. The station at HPP is offline

Fig. 8 Data availability of one channel at each station (the availability is consistent for all channels). Gaps are plotted as vertical red lines. The data are plotted as horizontal lines



HPP. Although the west side of the dam reservoir was very hard to access and the Georgia-Abkhazia border zone was an additional constraint in site selection, we installed one station (GULB) in the high mountain area (which takes about 10 h round-trip to reach the station with special truck); however, the real-time data transfer from that station did not work properly. The station in Abkhazia, HPP, was added to the initial network layout in October 2021 to increase the network coverage around the Gali reservoir.

4.1 Ambient noise level

To investigate the ambient noise level within the current seismic network and assess the impact of station depth on noise reduction, we conducted an analysis of background noise using probability power spectral densities (PPSDs) (McNamara and Buland 2004). Contin-

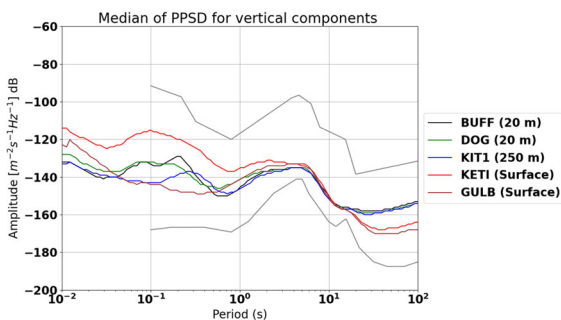


Fig. 9 Median values of PPSDs computed for vertical components of stations installed at different depths and locations over the year 2022. The two grey curves indicate the new high- and low-noise models (Peterson et al. 1993)

uous data recorded at each seismic station were utilized to compute the PPSDs. Figure 9 illustrates a comparison between five different stations in the study area, installed at different depths. The stations included in the comparison are KETI and GULB, which are located at the ground level, stations DOG and BUFF, installed at a depth of 20 m and the KIT1 which was installed in a 250-m borehole (see Fig. 7 for the station locations on the map). The visualization of the median PPSD for the vertical components offers valuable insights into the noise levels, signal quality, and spectral characteristics at different sensor's location and depth, enabling an assessment of the seismic network's performance and its suitability for various research and monitoring objectives. This may be crucial for making informed decisions about future seismic monitoring efforts in the region. According to the Fig. 9, KETI (red curve), exhibits the highest noise level across all frequency ranges, indicating this surface station is more susceptible to various sources affecting data quality. Station DOG and BUFF, both at 20 m depth, show similar noise levels below 3 Hz. However, above 3 Hz, there is a recognisable difference of up to 5 dB between them, suggesting that the local noise sources influence noise characteristics at higher frequencies. In the frequency range of approximately 3 to 25 Hz (period range between 0.03 and 0.3 s), KIT1 demonstrates the greatest noise level reduction compared to the shallow borehole stations, BUFF and DOG, with a decrease of about 10 dB. In the frequency band between about 2 and 6 Hz (period range 0.15 to 0.5 s), GULB, the surface station located in mountain, shows the lowest noise level compared to the other stations. The observed differences in noise levels at higher frequency bands are influenced by

a variety of factors. These factors include the installation of sensors in boreholes, the presence of cultural and anthropogenic noise, and various local geology beneath the stations. Borehole installations offer the advantage of providing a more stable and isolated environment, leading to reduced noise contamination and enhanced signal quality at higher frequencies. However, interestingly, station GULB, despite being installed at the surface, shows lower noise levels compared to other surface stations. This suggests that the noise reduction at station GULB could be attributed to its remote location far from anthropogenic noise sources and different geological characteristics of the ground between southern slope zone of the Caucasus mountain range and, for example, Rioni Basin (see Fig. 1), which has a significant impact on seismic noise levels measured at the ground level.

The findings presented in the figure have crucial implications for the design and implementation of the seismic network and monitoring strategies in the study area. The installation of sensors in boreholes has been demonstrated to offer significant benefits in reducing the impact of higher frequency noise sources, such as those originating from anthropogenic activities.

5 Recent seismicity around the Enguri dam

In this section, the seismicity recorded around Enguri dam by the newly installed seismic network is discussed. The aim has been to identify weak seismic events and to provide a preliminary location and magnitude estimation for events with clear P- and S-phases on at least three stations.

5.1 Event detection and location process

Event detection is performed in two steps. In the first step, the recorded continuous waveforms of all stations are scanned to extract the list of events with a high signal-to-noise ratio (SNR), that have occurred beneath the network. This step aims at identifying events generated at all major seismogenic zones (faults segments). Then, in the next step, the weaker events are extracted using the template matching technique, employing a subset of the events detected by the first step as templates. This two-step technique ensures that the weak seismicity related to the major local seismic sources

is extracted to compile an event catalog with a lower magnitude of completeness.

The first step is carried out using a source scan algorithm, namely the Lassie program (Heimann 2017), which is an automatic algorithm for detecting and locating earthquakes. This processing is based on migrating and stacking a characteristic function calculated from normalized amplitude envelopes measured at each station and to look for coherent arrivals of P- and S-waves at all stations (Adinolfi et al. 2019; Lopez-Comino et al. 2017; Matos et al. 2018). As a pre-processing step, the travel times for seismic phases are computed for a 3-D spatial grid of possible seismogenic zone using the CAKE tool (Heimann et al. 2017) and using a local 1-D velocity model (Murusidze 1987) (see Table 2). To make the 3-D spatial grids, a 15 km distance from the dam location and up to 50 km depth is assumed, accordingly, a $30 \times 30 \times 50$ km grid with 1 km grid spacing is searched for a possible earthquake location and an event is defined if the value of the characteristic function reaches a predefined threshold. The evaluation of coherency is done using continuous waveforms that are cut into overlapping time windows (width equal to 10 min with 20% overlap). The origin time of the detected earthquake is determined from the detected time, and travel time of the phases between the related grid location (trial earthquake hypocenter) and the reference point or station used for calculating the stacked characteristic function. A 10 to 40 Hz band-pass filter is applied to the raw data. We used higher weights for the P-phases and a detector threshold of 75 on the detector function. Figure 10 shows an example of a detected and located event using Lassie and explains the basic steps of the procedure. It should be noted that the network records seismicity outside of our zone of interest and most of them could be detected by Lassie with preliminary locations at the edges of the search grid. Accordingly, all detections from Lassie have been inspected visually, and only local events (according to arrival time differences of S- and P-phases) originating from sources beneath the network and in the zone of interest are kept.

In the second step, the template matching technique is employed to improve the detection capability of weak events (Gibbons and Ringdal 2006; Meng et al. 2018) that, due to low SNR, might not be detectable using detection techniques based on time-domain amplitude inspection. The waveforms of the events selected in the first step that exhibit a sufficient quantity of high-

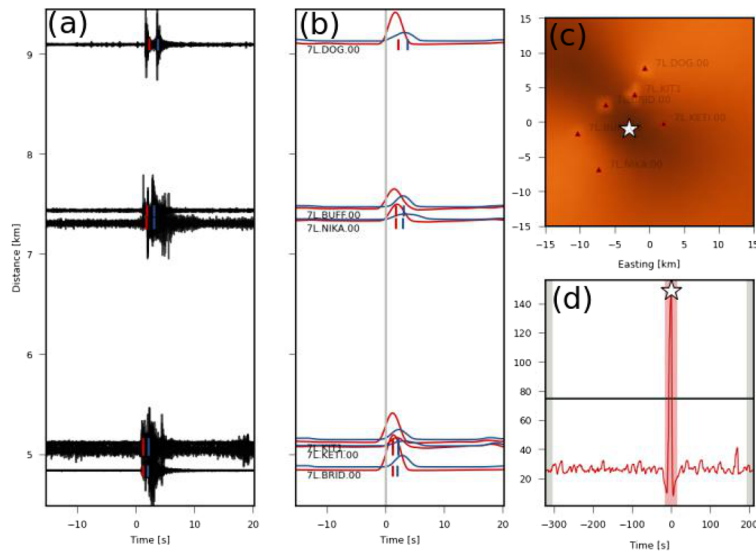


Fig. 10 Example of detection using Lassie. The origin time of the event is at 2022-03-16 10:07:38:112. **a** All available waveforms used for event detection and location are sorted by hypocentral distance (Band pass filter: 10–40 Hz). **b** Characteristic functions (normalized amplitude envelope) for each trace used for migration (based on P-wave (red lines), and S-wave (blue lines) theoretical arrival times) and stacking. **c** Coherence (stacked) map for all grid points (2D projection). Dark colors

show high coherence values. The location of the detected event is marked with the white star. Station locations are shown with black triangles. **d** Global detector level function in a processing time window centered around the origin time of the detected event. The cut-out time window used for the coherence map is shown in gray color. The white star indicates the detected event above the fixed threshold of 75 (black line)

quality phase picks are taken as templates. Then, scanning through the continuous waveform data, prior or posterior to the template timestamp is performed to find new similar events. The comparison of the template waveform and the piece of the signal under analysis is quantified by a correlation coefficient; detection is declared once the value of the correlation exceeds a predefined threshold. We used the EQcorrscan algorithm (Chamberlain et al. 2018) which is an open-source software package written in Python, for the detection and analysis of seismicity, on an eight-core computer. All detections have been inspected manually and detected events with high signal quality at more than three stations are imported into the SEISAN earthquake analysis software database (Havskov and Ottemöller 1999) for phase picking, location, and magnitude estimation. The P- and S-phase onset times are picked manually. For some strong events with high SNR moment magnitude, M_w is estimated as well, based on spectral analysis of S-phases on vertical component traces.

5.2 Observed seismicity

After analyzing the data recorded until the end of July 2022, over 448 local events were identified, with approximately 320 of them occurring within the area of interest, represented by the red square in Fig. 1. Figure 11 shows the observed seismicity map, where the circles are scaled by the estimated magnitude of events (all events below magnitude 0.0 are shown with the same scale) and the white circles are events with location uncertainty greater than 5 km in each principal direction. The colorbar illustrates focal depth of events in km. The seismicity pattern exhibits clustered events, particularly near the existing fault's location, as well as scattered events throughout the region. However, it is essential to consider the potential sources of location error, which may arise from various factors. These include azimuthal gap issues for events outside the monitoring network's footprint, limitations due to employing a 1-D velocity model to locate the seismic-

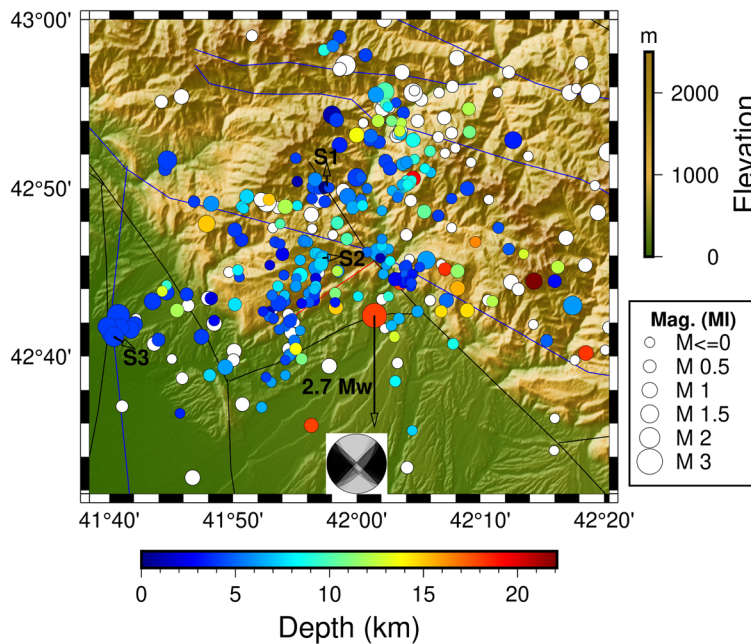


Fig. 11 Seismicity map obtained in this study using the local seismic network currently operating at Enguri site. White circles represent the events that are poorly located (error greater than 5 km in at least one of the hypocentral parameters). Scattered

seismicity as well as clusters close to the fault lines are observed, which are indicated by S1, S2, and S3. The focal mechanism of magnitude M_w 2.8 (M_l 2.7) event calculated in this study is shown

ity within a complex geological structure and under a strongly varying topographic area. Additionally, phase picking errors could occur, particularly in cases of low SNR. The histograms depicted in Fig. 12a and b illustrate the depth and magnitude distribution of the located events (red markers in Fig. 11). The majority of events occurred in a depth range between 4 and 8 km, with the peak occurrence at 4.1 km. It should be noted that the magnitude estimation for about 20 located events was not possible due to the low signal-to-noise ratio. Consequently, those events are not represented in the magnitude histogram. The observed drop in the number

of events with a magnitude of about 0.5 M_l compared to the cases above magnitude 0.7 M_l (see Fig. 12b) could be attributed to the fact that the magnitude of completeness is not uniform for entire region shown in Fig. 11, for seismological sources, such as those located at the north and east side of the study area, only stronger events are detected and are included in the histogram. In addition, we did not specifically look for weak events originating from the sources outside the 15 km radius from the dam (except events close to the Gali reservoir) using the template matching technique. The estimated magnitude of most events falls below M_l 1.0; how-

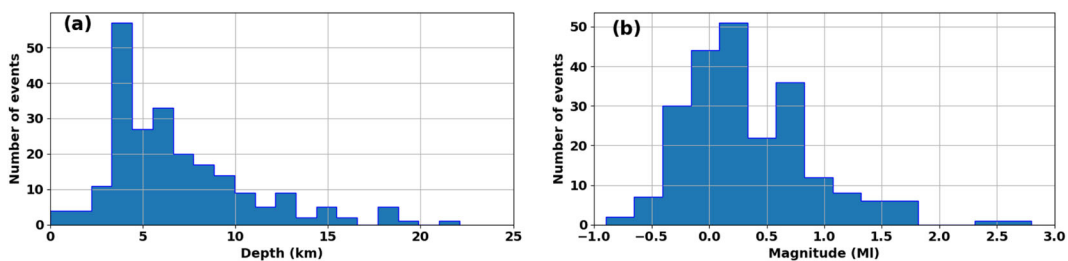


Fig. 12 Depth **a** and magnitude **b** distribution of the seismicity

ever, there were also two notable events with magnitude above M_l 2.0 that were recorded. (1) An event with a magnitude of M_l 2.4 (M_w 2.7) occurred on 2021-03-05 at 10:04 UTC. It took place at latitude, longitude, and depth of 42.707° , 41.679° , and 4.1 km, respectively. This event was approximately, 30km away from the dam, and about 10km from to the Gali reservoir. (2) The largest event recorded in the closer vicinity of the dam, with a magnitude of M_l 2.7 (M_w 2.8), occurred on 2022-02-01 at 21:33. It had a latitude, longitude, and depth of 42.707° , 42.024° , and 18 km, respectively. This event occurred at a distance of about 5 km from the dam.

Figure 13a illustrates the water level (black) and water level velocity (blue) of the Enguri dam reservoir since the local seismic network has started recording one complete cycle, that is releasing water from the reservoir, stabilizing it, filling the reservoir again and stabilizing it at a high-level, plus three from four stages of the following cycle happened during that period. Each

stage of water level change is labeled with a letter and the initial time of each one is indicated by a red vertical line. The water level changed in the first cycle by about 100 m during the releasing and the filling stages, i.e. stage (a) from October 2020 to February 2021 and stage (c) between March 2021 and June 2021. In the following cycle, stage (e) shows a water level drop of 80 m. From the plot, one can see that the low water stage is almost twice longer in the second cycle (stage f) than in the first one (stage b).

In Fig. 13b, the histogram presented in gray displays the weekly number of events above the catalog magnitude of completeness. As previously mentioned, the seismic network was completed during different time stages, and to reflect this, the number of active stations is plotted in blue in Fig. 13b, with the right-hand side axis. The magnitude of completeness for the catalog is determined to be M_l 0.5, during the time when four stations were operational. However, with the addition of four more stations and a total of eight stations in oper-

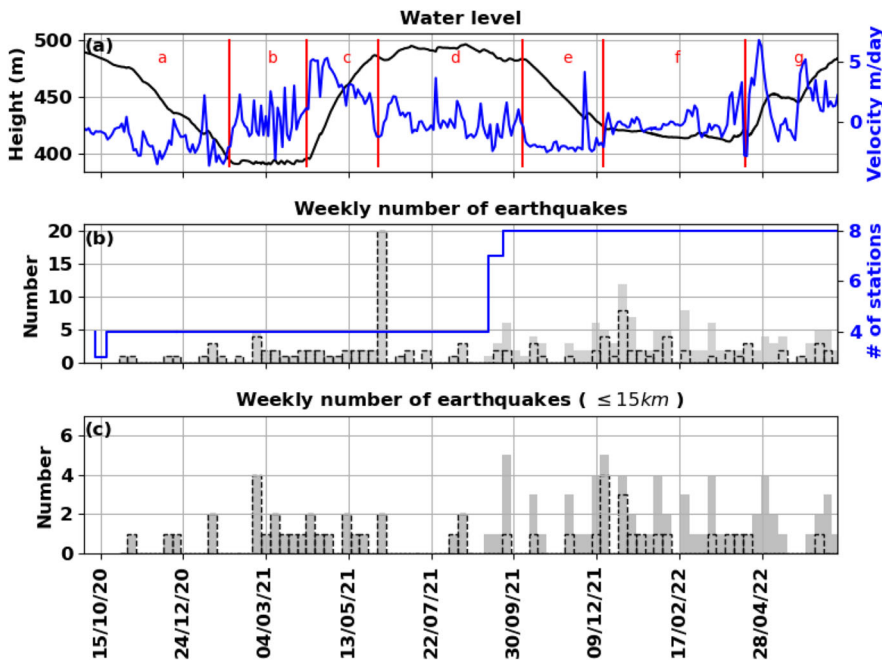


Fig. 13 Water level variation is plotted in black and the water speed (derivation of daily water level) is shown in blue color and right axes in panel (a). A Histogram of a weekly number of located events above an estimated magnitude of completeness is plotted in (b), and for events in 15 km horizontal distance from the dam in (c). The right axes plotted in blue in (b) shows the number of stations operating with time. The histogram plotted

with a dashed line is obtained by processing the events excluding the four stations added shortly before stage (d), in c only events at a 15 km distance from the dam are plotted. The initial timing of different stages of water level change is indicated by vertical red lines. The letters indicated on each stage are linked to the seismicity plot labels in Fig. 15

ation, the magnitude of completeness for the catalog is improved to M_I 0.0.

Based on this histogram, a sudden rise in the weekly number of earthquakes occurred during the seismicity monitoring period, which is observed in June 2021, in addition, after December 2021 (in stage f), the seismicity shows increases. In Fig. 13c, events with distances larger than 15 km from the Enguri dam are excluded from the catalog. A small rise is observed in February 2021, which shows the highest number of events with magnitude above M_I 0.5 up to the end of first water filling cycle (stage a–d).

Figure 13 evidences that there may be a correlation between the increase in observed seismic activity after stage (d) and the increase in number of stations in the monitoring network from four to eight stations. To ensure a fair comparison of seismicity across different stages, a careful analysis was conducted. Therefore, the recordings from the four stations added at the end of stage (d) were excluded from the event location process. The results of this analysis are shown in the second histogram, represented by a black dashed line

in Fig. 13b and c. In the latter case, there is a noticeable decrease in the number of observed seismic events per week and a total number of 76 events above the magnitude of completeness could not be located. However, despite the exclusion of the latest four stations in the event location process, the increase in seismicity is still noticeable in stage (f). This indicates that, the observed rise in seismic activity can not be solely attributed to the increased number of stations. It is worth noticing that, the largest observed seismic event in this study occurred in stage (f), with a magnitude of M_I 2.4. Additionally, two other events with magnitudes above M_I 1.4 were also recorded during the same stage. The first event, with a magnitude of M_I 1.4 (M_w 1.5), occurred on 2021-12-15 at 04:50 UTC. It was located at a latitude of 42.776° and a longitude of 42.029° , with a depth of 6.3 km. The event was the closest to the dam, at a distance of 2 km. The second event, with a magnitude of M_I 1.5 (M_w 1.9), occurred on 2021-03-18 at 02:24 UTC. It was located at a latitude of 42.762° and a longitude of 42.094° , with a depth of 6.2 km. The event was 5 km away from the dam.

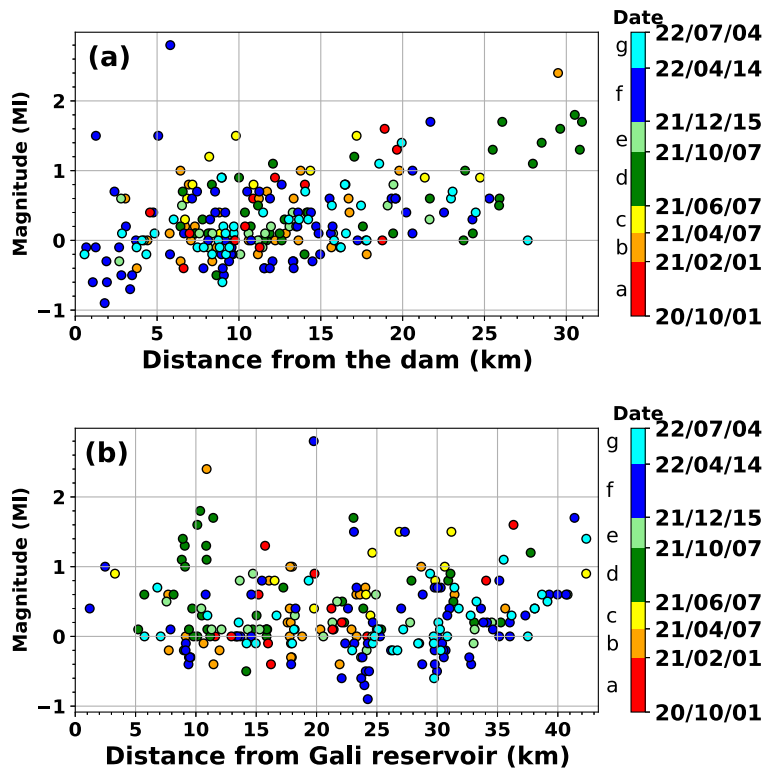


Fig. 14 Magnitude vs distance of the events calculated from **a** Enguri dam, **b** Gali reservoir. The color bar in each plot indicates to the origin time of the events and the date format is “year/month/day”

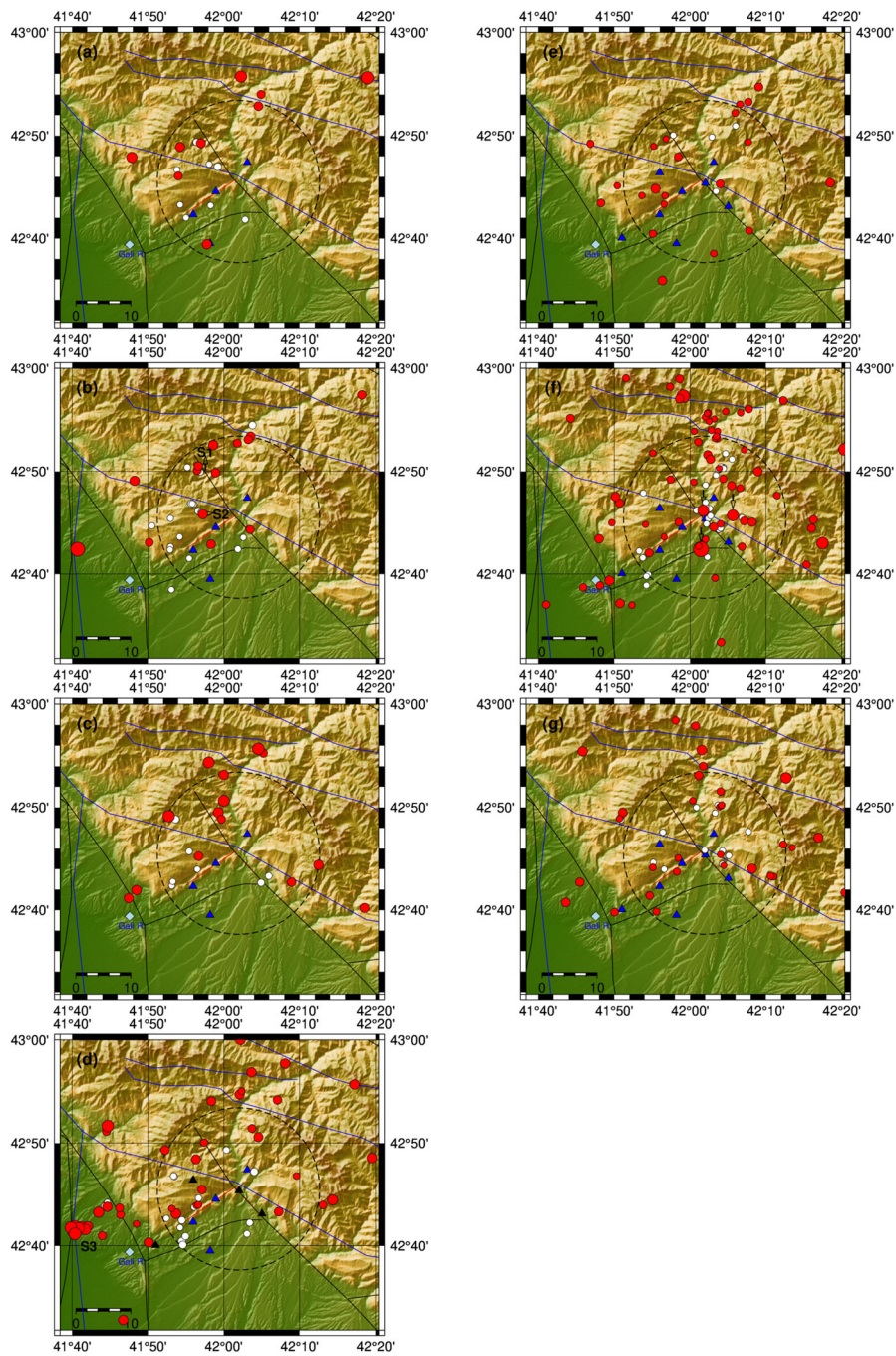


Fig. 15 Spatial pattern of seismicity at each stage of dam reservoir water level change are plotted in (a)–(g) (see Fig. 13 for the time span of each stage), red circles are events with a magnitude of greater than M_l 0.0 and white circles are events with magnitude below M_l 0.0. The black circle on each plot shows the 15 km distance from the dam, triangles show the seismic stations, while stations operating in the entire time span of each stage are plotted in blue. The black triangles in plot (a) and (d)

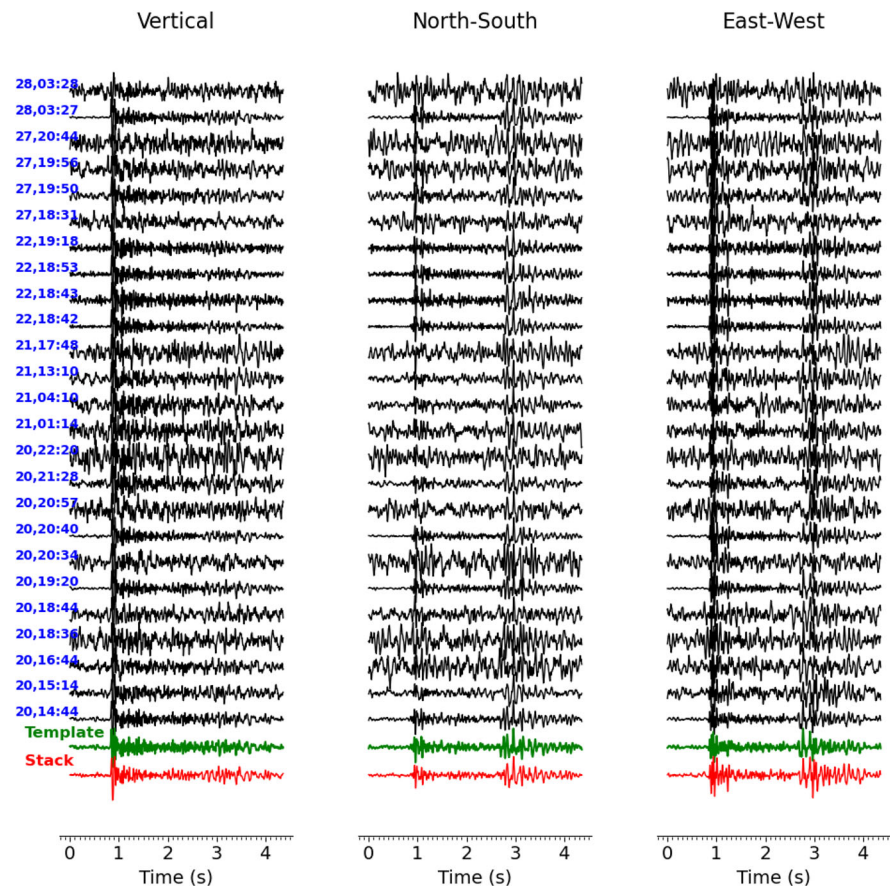
were operating partially, which in plot (a) is the station KIT1 that stopped operating shortly after the installation, and in plot (d) are stations added after September 2021. The fault lines in blue and black are previously introduced in Fig. 1. The locations of two seismic swarms observed in February 2021 are indicated in plot (b) by S1 and S2. The location of swarm occurred in June 2021 is indicated in plot (d) by S3. In plot (f) the location of events of magnitude above 1.4 are indicated by vertical small arrows

Figure 14a and b present the magnitude distribution of events plotted against the distance calculated from two reservoirs: the Enguri reservoir and the Gali reservoir. The colorbar in each plot represents the origin time of the events, with the time intervals discretely indicating the different stages of the Enguri reservoir water level changes as depicted in Fig. 13a. Figure 14a highlights that the network is sensible to recording weaker seismic events ($\leq M_l 0.0$) within a distance of about 15 km. However, within a closer proximity, up to 5 km from the dam, many events with magnitude below $M_l 0.0$ have been successfully identified and located. Most of these events are represented by the blue color, indicating their occurrence during later stages (f) and (g) of the water level cycle, in late 2021 and 2022. In this figure, a cluster of seismicity at about 8 km distance is noticeable as well, which includes events of magnitude ranging between -0.6 to about $M_l 1.0$. Figure 14b shows the nearest cluster of seismicity at about 10 km distance from the Gali reservoir. At this distance, while the seis-

micity observed in stages (d), in green color, appears to have a higher magnitude range, in the later stages of monitoring time, i.e., stage (f) in dark blue, weaker events are also observed.

The spatial distribution of seismicity related to the different stages of water level change is presented in the subplots of Fig. 15. Events with a magnitude greater than the magnitude of completeness (M_c) are represented in red color, while white circles are events with magnitude below M_c . In each subplot, triangles show the location of seismic stations, with blue color indicating stations that were operational throughout the entire stage and black color for stations that were only partly operational at the starting time (stage a) and latest time (stage d). Additionally, a black circle on each plot represents the 15 km distance range from the Enguri dam reservoir. The Ingirishi fault line is plotted in red, and the previously introduced faults in blue and black are also shown in Fig. 1. The plots highlight a scattered distribution of events around the Ingirishi fault during

Fig. 16 Waveforms of swarms including 25 events occurred in February 2021 recorded at station DOG, each plot shows one component traces. The numbers in the left plot represent the date of each event in day, hour:second format, the green and red traces at each plot show the template trace (the event occurred at 2021-02-22 18:43) and the stack of all detected events



all stages. However, in stage (d), when the water level stabilizes at a higher level, a distinct cluster of events is observed in close proximity to the fault. This clustering indicates to a higher seismicity rate during this stage, which may be attributed to the impact of reservoir water level change on the fault's behavior.

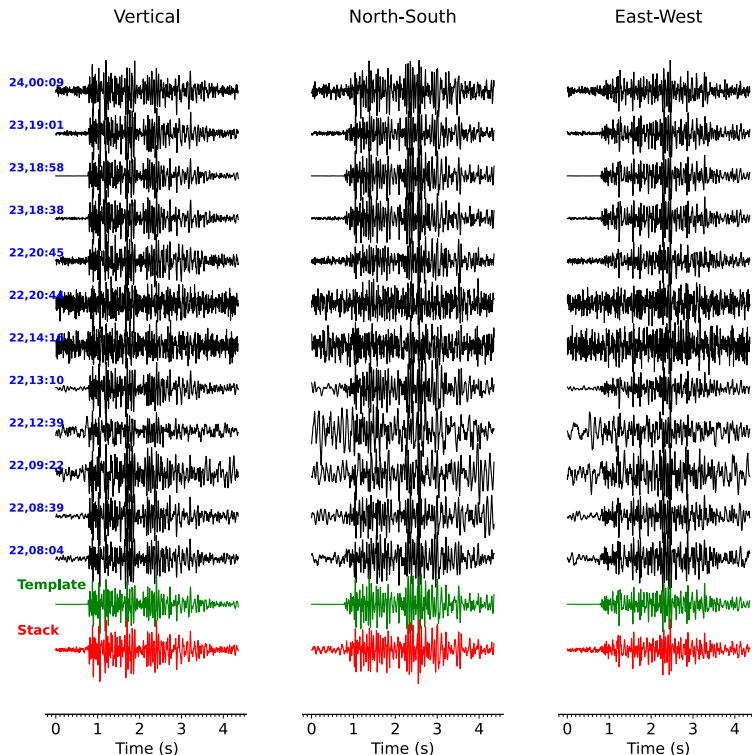
The observed temporal increase of seismicity in February 2021 (Fig. 15b) is related to two separated source locations or spatial clusters, according to the waveform similarity and the location of the biggest events in each sub-sequence. The larger cluster includes 3 relatively large events with magnitudes of M_l 0.7 (Feb. 28), M_l 0.6 (Feb. 20) and M_l 0.8 (Feb. 20), and occurred on the west side of the Enguri reservoir (marked on Fig. 15b with S1). This cluster consists of more than 25 detected events; however, just 5 of them could be located with an estimated magnitude range between M_l 0.0 and M_l 0.8. Figure 16 shows 3-component recordings of the events detected by the template matching technique at station DOG. The green waveforms in the figure show the template trace and the red traces show the linear stack of all traces. The observed time of each event is indicated on the left side of the figure on the vertical component waveform. The detected events are distributed in

8 days between 20 and 28 of February, in which 11 events occurred on February 20, 4 events on February 21, 4 on February 22, 4 on February 27, and 2 on February 28.

The other cluster includes one event with magnitudes M_l 1 (Feb 23) that occurred close to the Ingirishi fault (marked in Fig. 15b with S2), and the nearest recording station was BRID. This cluster includes 15 detected events, 11 of which could be located, the estimated magnitude range of those events is -1.3 to M_l 1.0 (see Fig. 17 for the waveforms at station BRID). The observed seismicity is distributed between February 22 and February 24, 8 events on February 22, 3 events on February 23, and 1 event on February 24.

Figures 15b and 11 show the location of the aforementioned clusters on the western side of the dam, one close to the Vartsikhe-Gegechkori fault passing through the dam and the other one along the Gagra-Java active fault in the northern side of the Ingirishi fault. Seismicity pattern in stage (c) is plotted in Fig. 15c, comparing with Fig. 15b, we see that earthquakes continue to occur in the same spot where two swarms were located. The increase of seismicity in stage (d) is mostly related to the events originated from the active zone close to

Fig. 17 Waveforms of swarms including 13 events occurred in February 2021 recorded at station BRID, each plot shows one component traces. The numbers in the left plot represent the date of each event in day, hour:second format, the green and red traces at each plot show the template trace (the event occurred at 2021-02-23 18:58) and the stack of all detected events



the Gali reservoir (see Fig. 15d). The interesting feature in this stage is the occurrence of a swarm on June 7, 2021, where 23 events are detected in about 8 min, 16 of them are located with a magnitude range between M_l 0.3 and M_l 1.8, and 10 events with a magnitude greater than M_l 0.1. The magnitude of the largest event in the sequence is M_l 1.8 (M_w 2.0). Figure 18 shows waveforms of the related events recorded in the station BRID. On 2021-03-05 at 10:04 a magnitude of M_l 2.4, M_w 2.7 occurred in the same location (see Fig. 15b). The seismicity related to the stage (f) is shown in Fig. 15f and appears as small clusters which are mostly distributed on the eastern side of the dam, on the Vartsikhegechkori active fault. Seismic activity is also observed along the prolongation of the Ingirishi fault to the SW to the Gali reservoir. That gives us a point to extend Ingirishi fault in this direction. The epicenter of three

big events ($M_l \geq 1.4$) in the close vicinity of the dam (introduced before) is indicated on the map.

5.3 Fault plane solution

From the recent observed seismicity, regarding the magnitude of the events and azimuthal coverage of events, the focal mechanisms of two events could be calculated. The biggest event with magnitude M_w 2.8 (M_l 2.7) took place at the Gagra-Java transpressional active faults (Fig. 11). This event occurred inside the recent local network, the mechanism estimated using first motion polarities and S- to P- phase amplitude ratio (Hardebeck and Shearer 2002) from all 8 available stations, is stable and indicates left-lateral strike-slip faulting (strike, dip and rake angles are 133° , 72° ,

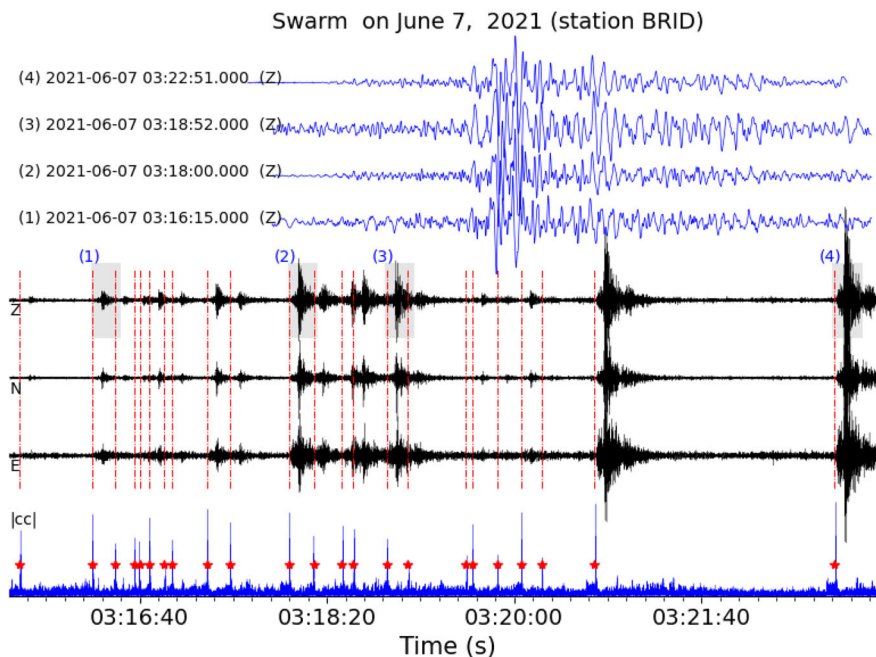


Fig. 18 Waveforms of the swarm occurred in June 7, 2021 recorded at station BRID, including 23 events in about 8 min time (bandpass filter: 2–18 Hz). Horizontal axis shows the time in the related day, where the format is hh:mm:ss. The 3 components recordings are plotted in black with Z, N, E for vertical, north–south and east–west components. Vertical red dashed lines show the timing of each detection using template matching technique, among them 4 detections are indicated by numbers 1–4 (event number 4 is the template event) and are plotted in a zoomed

window on top (blue traces). The gray area show the time span of each event (only vertical component) that is plotted in the zoomed window. The bottom plot in blue shows absolute value of the cumulative cross correlation (cc) of the template event with corresponding time segment, where the instants that cc stay above the predefined threshold (here MAD 9) are indicated by red stars (at the same timing as the red vertical dashed lines on the 3 components waveforms)

and -177° , respectively.) The fault plane strikes, in the NE-SW direction, is in agreement with the Gagra-Java active faults. Another event with M_w 1.5 (M_l 1.6) took place at the junction of two active faults. One of them is the Ingrishi fault and the other is either the Vartsikhe-Gegechkori (number 1 in Fig. 1a) right lateral - reverse active faults by Caputo et al. (2000) or the Mukhuri reverse fault (Adamia et al. 2008, 2010). The network coverage from the north side of this event is nonetheless weak, with two stations with compressional first motion polarities, whereas all the stations in the south recorded dilatational first motion polarity. The best fitted solution has strike, dip, and rake of 344° , 21° , and -8° , respectively; however, strike, dip, and rake of 128° , 6° , and 136° is the second possible solution. Accordingly, the possible solution is not unique and could be a strike-slip (with slightly different strikes) and oblique components.

6 Conclusion

On-going seismic monitoring shows that the study area is seismically active, and we could identify some local sources of seismicity. In particular, we observed that the Ingrishi fault, which was one of the monitoring targets in this study, generates microseismicity and we conclude that it is a seismically active fault. Ingrishi fault was not recognized as an active fault by Caputo et al. (2000) and Adamia et al. (2008, 2017). In addition, we observed seismicity along the prolongation of the Ingrishi fault which implies the extension of the fault to the SW direction. Unfortunately, this part cannot be investigated by geologists to understand how the fault can be extended to this direction, because of political reasons. Moreover, seismicity occurs with irregular time distribution as well as in temporal and spatial clusters, i.e., seismic swarms. One distinct seismic swarm, which occurred in the Gali reservoir region in June 2021, and several time-spatial clusters are observed in the recent seismicity pattern. The faults passing the dam are active with the possibility of generating earthquakes above M_l 1.5 at a distance close to the dam structure. Furthermore, comparing the old and recent seismicity of the region, we see the consistency of the location of some of the active sources, for instance, both Figs. 11 and 4 indicate high seismicity of the eastern part of the Utviri Fault passing through the Enguri dam, at the

boundary of the Main Range Zone and the Southern Slope Zone of the Great Caucasus. In addition, the other boundary of two main tectonic units, close to the Gali reservoir, also shows high seismicity in both catalogs. The depth distribution of the current and old seismicity highlights the 4 km depth as the most frequent shallow depth, while the depth of the biggest event (Mag M_w 2.8, 2022-01-02) is 18 km in agreement with the depth distribution observed in the old catalog (less than 20 km), considering the fact that the majority of old catalog events are of magnitude greater than M_w 2.0.

The epicentral location of the biggest event is close to the Gagra-Java transpressional active fault, and the focal mechanism solution concluded left-lateral strike-slip faulting, where the slipped fault plane strike is in NE-SW direction and in agreement with the Gagra-Java active fault.

The seasonal change that is observed in recent activities of the area and Ingrishi fault could be the natural behavior of the faults or possibly influenced by water level change in the dam reservoir. To conclude on this point, it is, however, necessary to monitor the seismicity over a longer time period and more cycles of dam reservoir water level change.

Based on background noise analysis, it becomes evident that a well-designed seismic network with a combination of borehole and surface installations, placed strategically with respect to noise sources, can significantly improve the accuracy and reliability of seismic data.

The local network is still running and the data processing will be carried on to provide more resources to better investigate the possible correlation between seismicity and dam reservoir water level change and to characterize the seismological behavior of the active fault segments.

Acknowledgements We are grateful to the anonymous reviewers for their constructive feedback, which contributed to the improvement of this manuscript. We would also like to extend our appreciation to the editor for the guidance and support throughout the review process. We are very grateful to Dr. Michael Fritsch and Felix Bögelspacher for their invaluable technical support throughout the course of the field work and supporting the operation of seismic network in this project.

Author contributions N.K did the data analysis of recent seismic network. N.K and N.T wrote the main manuscript text N.T and T.Sh did data processing of the old catalog All authors were involved in field trips and seismic network installations. All authors reviewed the manuscript.

Funding Open Access funding enabled and organized by Projekt DEAL. This study is funded by DAMAST and DAMAST-Transfer projects which are part of the “CLIENT II - International Partnership for Sustainable Innovations” funding program of the Federal Ministry of Education and Research (BMBF) of Germany within the framework program of “Research for Sustainable Development (FONA),” with project reference number of BMBF-Project 03G0882A (project website: <https://www.damast-caucasus.de/68.php>). This study is also partly funded by Shota Rustaveli National Science Foundation of Georgia, project number FR-21-20840.

Availability of data and material The Enguri current seismic network is registered with International Federation of Digital Seismograph Networks (FDSN) under network code 7L (https://fdsn.org/networks/detail/7L_2020/). The seismic catalog used in this study is publicly available at the KIT open library Repository (<https://publikationen.bibliothek.kit.edu/1000156936>) Karamzadeh Toularoud et al. (2023). The background seismic noise PPSD’s for all stations of Enguri current network are available to download internally from Geophysical Institute (GPI) of Karlsruhe Institute of Technology (KIT) website and can be provided upon request. For updated old seismic catalog of Enguri region please contact Dr. Nino Tsereteli.

Declarations

Ethical approval Not applicable

Conflict of interest The authors declare no competing interests.

Open Access This article is licensed under a Creative Commons Attribution 4.0 International License, which permits use, sharing, adaptation, distribution and reproduction in any medium or format, as long as you give appropriate credit to the original author(s) and the source, provide a link to the Creative Commons licence, and indicate if changes were made. The images or other third party material in this article are included in the article’s Creative Commons licence, unless indicated otherwise in a credit line to the material. If material is not included in the article’s Creative Commons licence and your intended use is not permitted by statutory regulation or exceeds the permitted use, you will need to obtain permission directly from the copyright holder. To view a copy of this licence, visit <http://creativecommons.org/licenses/by/4.0/>.

References

- Adamia SA, Chkhotua T, Kekelia M, Lordkipanidze M, Shavishvili I, Zakariadze G (1981) Tectonics of the Caucasus and adjoining regions: implications for the evolution of the Tethys ocean. *J Struct Geol* 3(4):437–447
- Adamia S, Mumladze T, Sadradze N, Tsereteli E, Tsereteli N, Varazanashvili O (2008) Late cenozoic tectonics and geodynamics of Georgia (SW Caucasus). *Georgian Int J Sci Technol* 1:77–107
- Adamia S, Alania V, Chabukiani A, Chichua G, Enukidze O, Sadradze N (2010) Evolution of the late cenozoic basins of

- Georgia (SW Caucasus): a review. *Geol Soc London Spec Publ* 340(1):239–259
- Adamia S, Alania V, Tsereteli N, Varazanashvili O, Sadradze N, Lursmanashvili N, Gventsadze A (2017) Postcollisional tectonics and seismicity of Georgia. Tectonic evolution, collision, and seismicity of southwest Asia: in honor of Manuel Berberian’s forty-five years of research contributions. *Geol Soc Am Spec Pap* 525:535–572
- Adinolfi G, Cesca S, Picozzi M, Heimann S, Zollo A (2019) Detection of weak seismic sequences based on arrival time coherence and empiric network detectability: an application at a near fault observatory. *Geophys J Int* 218(3):2054–2065
- Aktuğ B, Meherremov E, Kurt M, Özdemir S, Esedov N, Lenk O (2013) GPS constraints on the deformation of Azerbaijan and surrounding regions. *J Geodyn* 67:40–45
- Alizadeh AA, oğly Guliyev IS, Kadirov FA, Eppelbaum LV (2016) *Geosciences of Azerbaijan*, Springer, volume 1
- Allen MB, Vincent SJ, Alsop GI, Ismail-zadeh A, Flecker R (2003) Late cenozoic deformation in the South Caspian region: effects of a rigid basement block within a collision zone. *Tectonophysics* 366(3–4):223–239
- Allen M, Jackson J, Walker R (2004) Late cenozoic reorganization of the Arabia-Eurasia collision and the comparison of short-term and long-term deformation rates. *Tectonics* 23(2)
- Avagyan A, Sosson M, Karakhanian A, Philip H, Rebai S, Roland Y, Melkonyan R, Davtyan V (2010) Recent tectonic stress evolution in the lesser Caucasus and adjacent regions. *Geol Soc London Spec Publ* 340(1):393–408
- Axen GJ, Lam PS, Grove M, Stockli DF, Hassanzadeh J (2001) Exhumation of the west-central Alborz Mountains, Iran, Caspian subsidence, and collision-related tectonics. *Geology* 29(6):559–562
- Banks CJ, Robinson AG, Williams MP (1998) Structure and regional tectonics of the Achara-Trialet fold belt and the adjacent Rioni and Kartli foreland basins, Republic of Georgia. *Mem Am Assoc Pet Geol* 331–346
- Berberian M, Yeats RS (1999) Patterns of historical earthquake rupture in the Iranian Plateau. *Bull Seismol Soc Am* 89(1):120–139
- Braun T, Cesca S, Kühn D, Martirosian-Janssen A, Dahm T (2018) Anthropogenic seismicity in Italy and its relation to tectonics: state of the art and perspectives. *Anthropocene* 21:80–94
- Caputo M, Gamkrelidze I, Malvezzi V, Sgrigna V, Shengelaia G, Zilpimiani D (2000) Geostructural basis and geophysical investigations for the seismic hazard assessment and prediction in the Caucasus. *Il Nuovo Cimento C* 23(2):191–216
- Chamberlain CJ, Hopp CJ, Boese CM, Warren-Smith E, Chambers D, Chu SX, Michailos K, Townend J (2018) EQcorrscan: repeating and near-repeating earthquake detection and analysis in python. *Seismol Res Lett* 89(1):173–181
- Chelidze T, Matcharashvili T, Abashidze V, Dovgal N, Mepharidze E, Chelidze L (2019) Nonlinear dynamics of seismicity and fault zone dynamics around large dams: the case of Enguri dam, Caucasus. *Multidiscip Digit Publ Inst Proc* 24(1):28
- Chelidze T, Matcharashvili T, Abashidze V, Dovgal N, Mepharidze E, Chelidze L (2021) Time series analysis of fault strain accumulation around large dam: the case of Enguri dam,

- greater Caucasus. In: Building knowledge for geohazard assessment and management in the Caucasus and other orogenic regions, Springer, pp 185–204
- DeMets C, Gordon RG, Argus D, Stein S (1990) Current plate motions. *Geophys J Int* 101(2):425–478
- DeMets C, Gordon RG, Argus DF, Stein S (1994) Effect of recent revisions to the geomagnetic reversal time scale on estimates of current plate motions. *Geophys Res Lett* 21(20):2191–2194
- Dewey JF, PITMAN III WC, Ryan WB, Bonnin J, (1973) Plate tectonics and the evolution of the Alpine system. *Geol Soc Am Bull* 84(10):3137–3180
- Gamkrelidze PD (1966) Tectonic of Georgia. *Geology of USSR* 10(part I):9–21
- Gibbons SJ, Ringdal F (2006) The detection of low magnitude seismic events using array-based waveform correlation. *Geophys J Int* 165(1):149–166
- Guliev I, Kadirov F, Reilinger R, Gasanov R, Mamedov A (2002) Active tectonics in Azerbaijan based on geodetic, gravimetric, and seismic data. *Doklady earth sciences c/c of Doklady-Akademiia Nauk, INTERPERIODICA PUBLISHING* 383:174–177
- Gupta HK (1992) Reservoir induced earthquakes. Elsevier
- Hardebeck JL, Shearer PM (2002) A new method for determining first-motion focal mechanisms. *Bull Seismol Soc Am* 92(6):2264–2276
- Havskov J, Ottemöller L (1999) SEISAN earthquake analysis software. *Seismol Res Lett* 70(5):532–534
- Heimann S (2017) Lassie, a friendly earthquake detector. <https://git.pyrocko.org/pyrocko/lassie.git>
- Heimann S, Kriegerowski M, Isken M, Cesca S, Daout S, Grigoli F, Juretzek C, Megies T, Nooshiri N, Steinberg A et al (2017) Pyrocko-an open-source seismology toolbox and library
- Jackson J, McKenzie D (1988) The relationship between plate motions and seismic moment tensors, and the rates of active deformation in the Mediterranean and Middle East. *Geophys J Int* 93(1):45–73
- Jackson J, Ambraseys N, Giardini D, Balassanian S (1997) Convergence between Eurasia and Arabia in eastern Turkey and the Caucasus. *Historical and Prehistorical Earthquakes in the Caucasus* 28:79–90
- Kadirov F, Mammadov S, Reilinger R, McClusky S (2008) Some new data on modern tectonic deformation and active faulting in Azerbaijan (according to Global Positioning System measurements). *Azerbaijan Natl Acad Sci Proc Sci Earth* 1:82–88
- Kadirov F, Floyd M, Reilinger R, Alizadeh AA, Guliyev I, Mammadov S, Safarov R (2015) Active geodynamics of the Caucasus region: implications for earthquake hazards in Azerbaijan. *Proc Azerbaijan Natl Acad Sci, Sci Earth* 3:3–17
- Kadirov F, Gadirov A, Abdullayev N (2012) Gravity modelling of the regional profile across South Caspian basin and tectonic implications. *The Modern Problems of Geology and Geophysics of Eastern Caucasus and the South Caspian Depression* 231:251. Nafta-Press, Baku
- Karamzadeh Toularoud N, Gaucher E, Tsereteli N, Frietsch M, Bögelspacher F, Tugushi N, Shubladze T, Rietbrock A (2023) Enguri Catalog KIT (version 2023-03-14). KIT open repository
- Khain V (1975) Structure and main stages in the tectono-magmatic development of the Caucasus: an attempt at geodynamic interpretation. *Am J Sci* 275:131–156
- Koçyiğit A, Yilmaz A, Adamia S, Kuloshvili S (2001) Neotectonics of east Anatolian plateau (Turkey) and lesser Caucasus: implication for transition from thrusting to strike-slip faulting. *Geodin Acta* 14(1–3):177–195
- Lee W (1975) A computer program for determining hypocenter, magnitude, and first motion pattern of local earthquakes. *US Geol Surv Open File Report* 75(311):1–116
- Lopez-Comino JA, Cesca S, Heimann S, Grigoli F, Milkereit C, Dahm T, Zang A (2017) Characterization of hydraulic fractures growth during the äspö hard rock laboratory experiment (Sweden). *Rock Mech Rock Eng* 50(11):2985–3001
- Martin RJ, Gulen L, Sun Y, Toksoz M (2010) The crustal and mantle velocity structure in central Asia from 3D travel time tomography. Technical report, New England research Inc (Veterans Affairs) white river junction Vt
- Mastitsky AK, Jigauri GM, KS (1974) Engineer- geological peculiarities of EHEPS Arc dam foundation. 6(8):3–6
- Matcharashvili T, Telesca L, Chelidze T, Javakhishvili Z, Zhukova N (2013) Analysis of temporal variation of earthquake occurrences in Caucasus from 1960 to 2011. *Tectonophysics* 608:857–865
- Matos C, Custódio S, Batló J, Zahradník J, Arroucau P, Silveira G, Heimann S (2018) An active seismic zone in intraplate West Iberia inferred from high-resolution geophysical data. *J. Geophys. Res. Solid Earth* 123(4):2885–2907
- Mcclusky S, Balassanian S, Barka A, Demir C, Ergintav S, Georgiev I, Gurkan O, Hamburger M, Hurst K, Kahle H et al (2000) Global positioning system constraints on plate kinematics and dynamics in the eastern Mediterranean and Caucasus. *J Geophys Res Solid Earth* 105(B3):5695–5719
- McNamara DE, Buland RP (2004) Ambient noise levels in the continental United States. *Bull Seismol Soc Am* 94(4):1517–1527
- Meng X, Chen H, Niu F, Tang Y, Yin C, Wu F (2018) Micro-seismic monitoring of stimulating shale gas reservoir in SW China: 1 an improved matching and locating technique for downhole monitoring. *J Geophys Res Solid Earth* 123(2):1643–1658
- Mosar J, Kangarli T, Bochud M, Glasmacher UA, Rast A, Brunet M-F, Sosson M (2010) Cenozoic-recent tectonics and uplift in the greater Caucasus: a perspective from Azerbaijan. *Geol Soc Spec Publ* 340(1):261–280
- Murusidze G (1987) Velocity model of the upper mantle in Caucasus and adjacent region. Mecniereba Publishing Office, Tbilisi (133 pages)
- Murusidze GY (1980) Seismicity and the possible position of strong earthquakes sources in the area of the Inguri HPP. In: Savarensky EF (ed) Seismic impacts on hydrotechnical and power structures. Moscow, Pub, House Nauka, pp 73–80
- Murusidze GY, Lursmanashvili OV (1962) On the study of the elastic properties of rocks. *Proc Inst Geophys AS GSSR* 20:113–133
- Okay AI, Sahinturk O (1997) Aapg Memoir 68: regional and petroleum geology of the black sea and surrounding region. Chapter 15: geology of the Eastern Pontides

- Onur T, Gok R, Godoladze T, Gunia I, Boichenko G, Buzaladze A, Tumanova N, Dzmanashvili M, Sukhishvili L, Javakishvili Z et al (2019) Probabilistic seismic hazard assessment for Georgia. Technical report, Lawrence Livermore National Lab.(LLNL), Livermore, CA (United States)
- Papalashvili V (1981) Development of the network of seismic stations in the Caucasus and some issues of generalization of observational material. *Seismological bulletin of the Caucasus*, Tbilisi 1978, Metsniereba Publ. House, pp 244–279
- Pasquarè F, Tormey D, Vezzoli L, Okrostsvardidze A, Tutberidze B (2011) Mitigating the consequences of extreme events on strategic facilities: evaluation of volcanic and seismic risk affecting the caspian oil and gas pipelines in the republic of Georgia. *J Environ Manag* 92(7):1774–1782
- Pearce JA, Bender J, De Long S, Kidd W, Low P, Güner Y, Saroglu F, Yilmaz Y, Moorbath S, Mitchell J (1990) Genesis of collision volcanism in Eastern Anatolia. Turkey. *J Volcanol Geotherm Res* 44(1–2):189–229
- Peinke J, Matcharashvili T, Chelidze T, Gogishvili J, Nawroth A, Lursmanashvili O, Javakishvili Z (2006) Influence of periodic variations in water level on regional seismic activity around a large reservoir: field data and laboratory model. *Phys Earth Planet Inter* 156(1–2):130–142
- Peterson J et al (1993) Observations and modeling of seismic background noise, US Geological Survey Reston, VA, USA, vol 93
- Philip H, Cisternas A, Gvishiani A, Gorshkov A (1989) The Caucasus: an actual example of the initial stages of continental collision. *Tectonophysics* 161(1–2):1–21
- Rautian T (1964) Determination of earthquake energy at a distance to 3000 km. *Eksp Seismika Trudy IFZ AN SSSR* 32:199
- Rebai S, Philip H, Dorbath L, Borissoff B, Haessler H, Cisternas A (1993) Active tectonics in the lesser Caucasus: coexistence of compressive and extensional structures. *Tectonics* 12(5):1089–1114
- Reilinger R, McClusky S, Oral M, King R, Toksoz M, Barka A, Kinik I, Lenk O, Sanli I (1997) Global positioning system measurements of present-day crustal movements in the Arabia-Africa-Eurasia plate collision zone. *J Geophys Res Solid Earth* 102(B5):9983–9999
- Reilinger R, McClusky S, Vernant P, Lawrence S, Ergintav S, Cakmak R, Ozener H, Kadirov F, Guliev I, Stepanyan R et al (2006). GPS constraints on continental deformation in the Africa-Arabia-Eurasia continental collision zone and implications for the dynamics of plate interactions. *J Geophys Res Solid Earth* 111(B5)
- Shevchenko V, Guseva T, Lukk A, Mishin A, Prilepin M, Reilinger R, Hamburger M, Shempelev A, Yunga S (1999) Recent geodynamics of the Caucasus mountains from GPS and seismological evidence. *Izv Phys Solid Earth* 35(9):691–704
- Smith AG (1971) Alpine deformation and the oceanic areas of the Tethys, Mediterranean, and Atlantic. *Geol Soc Am Bull* 82(8):2039–2070
- Sokhadze G, Floyd M, Godoladze T, King R, Cowgill E, Javakishvili Z, Hahubia G, Reilinger R (2018) Active convergence between the lesser and greater Caucasus in Georgia: constraints on the tectonic evolution of the lesser-greater caucasus continental collision. *Earth Planet Sci Lett* 481:154–161
- Sosson M, Rolland Y, Müller C, Danelian T, Melkonyan R, Kekeilia S, Adamia S, Babazadeh V, Kangarli T, Avagyan A et al (2010) Subductions, obduction and collision in the lesser Caucasus (Armenia, Azerbaijan, Georgia), new insights. *Geol Soc Spec Publ* 340(1):329–352
- Stabile TA, Giocoli A, Lapenna V, Perrone A, Piscitelli S, Telesca L (2014) Evidence of low-magnitude continued reservoir-induced seismicity associated with the Pertusillo artificial lake (southern Italy). *Bull Seismol Soc Am* 104(4):1820–1828
- Tan O, Taymaz T (2006) Active tectonics of the Caucasus: earthquake source mechanisms and rupture histories obtained from inversion of teleseismic body waveforms. *Spec Pap Geol Soc Am* 409:531
- Telesca L, Matcharashvili T, Chelidze T, Zhukova N (2012) Relationship between seismicity and water level in the Enguri high dam area (Georgia) using the singular spectrum analysis. *Nat Hazards Earth Syst Sci* 12(8):2479–2485
- Telesca L, Matcharashvili T, Chelidze T, Zhukova N, Javakishvili Z (2015) Investigating the dynamical features of the time distribution of the reservoir-induced seismicity in Enguri area (Georgia). *Nat Hazards* 77(1):117–125
- Tibaldi A, Alania V, Bonali F, Enukidze O, Tsereteli N, Kvavadze N, Varazanashvili O (2017) Active inversion tectonics, simple shear folding and back-thrusting at Rioni Basin, Georgia. *J Struct Geol* 96:35–53
- Tibaldi A, Russo E, Bonali F, Alania V, Chabukiani A, Enukidze O, Tsereteli N (2017) 3-d anatomy of an active fault-propagation fold: a multidisciplinary case study from Tsaishi, western Caucasus (Georgia). *Tectonophysics* 717:253–269
- Tibaldi A, Bonali F, Russo E, Mariotto FP (2018) Structural development and stress evolution of an arcuate fold-and-thrust system, southwestern greater Caucasus, republic of Georgia. *J Asian Earth Sci* 156:226–245
- Tibaldi A, Oppizzi P, Gierke JS, Oommen T, Tsereteli N, Odilavadze D (2018) Landsliding near Enguri dam (Caucasus. *Nat Hazards Earth Syst Sci*, Georgia) and possible seismoectonic effects
- Tibaldi A, Tsereteli N, Varazanashvili O, Babayev G, Barth A, Mumladze T, Bonali F, Russo E, Kadirov F, Yetirmishli G et al (2020) Active stress field and fault kinematics of the greater Caucasus. *J Asian Earth Sci* 188:104108
- Tibaldi A, Babayev G, Bonali FL, Pasquarè Mariotto F, Russo E, Tsereteli N, Corti N (2021) Active kinematics of the greater Caucasus from seismological and GPS data: a review. *Build Knowl for Geohazard Assess Manag in the Caucasus and other Orogenic Regions* 33–57
- Triep E, Abers G, Lerner-Lam AL, Mishatkin V, Zakharchenko N, Starovoit O (1995) Active thrust front of the greater Caucasus: the April 29, 1991, Racha earthquake sequence and its tectonic implications. *J Geophys Res Solid Earth* 100(B3):4011–4033
- Tsereteli N, Tanircan G, Safak E, Varazanashvil O, Chelidze T, Gvencadze A, Goguadze N (2012) Seismic hazard assessment for southern Caucasus-eastern turkey energy corridors: the example of Georgia. *Correl Hum Factors Prev Disasters* 94:96–111
- Tsereteli N, Askan A, Hamzehloo H (2016) Hybrid-empirical ground motion estimations for Georgia. *Acta Geophys* 64(5):1225–1256

- Tsereteli N, Tibaldi A, Alania V, Gventsadse A, Enukidze O, Varazanashvili O, Müller B (2016) Active tectonics of central-western Caucasus, Georgia. *Tectonophysics* 691:328–344
- Varazanashvili O, Tsereteli N, Bonali F, Arabidze V, Russo E, Pasquaré Mariotto F, Gogoladze Z, Tibaldi A, Kvavadze N, Oppizzi P (2018) GeoInt: the first macroseismic intensity database for the republic of Georgia. *J Seismol* 22(3):625–667
- Varazanashvili O, Tsereteli N, Tsereteli E et al (2011) Historical earthquakes in Georgia (up to 1900): source analysis and catalogue compilation
- Vincent SJ, Allen MB, Ismail-Zadeh AD, Flecker R, Foland KA, Simmons MD (2005) Insights from the Talysh of Azerbaijan into the Paleogene evolution of the South Caspian region. *Geol Soc Am Bull* 117(11–12):1513–1533
- Yilmaz Y, Tuysuz O, Yigitbas E, Genc SC, Sengor A (1997) AAPG memoir 68: regional and petroleum geology of the black sea and surrounding region. Chapter 11: Geology and Tectonic Evolution of the Pontides
- Zare M, Amini H, Yazdi P, Sesetyan K, Demircioglu MB, Kalafat D, Erdik M, Giardini D, Khan MA, Tsereteli N (2014) Recent developments of the middle east catalog. *J Seismol* 18:749–772

Publisher's Note Springer Nature remains neutral with regard to jurisdictional claims in published maps and institutional affiliations.